Drouet, S., Cotton, F. (2015): Regional Stochastic GMPEs in Low-Seismicity Areas: Scaling and Aleatory Variability Analysis—Application to the French Alps. - *Bulletin of the Seismological Society of America*, *105*, 4, p. 1883-1902.

DOI: http://doi.org/10.1785/0120140240

Bulletin of the Seismological Society of America, Vol. 105, No. 4, pp. 1883–1902, August 2015, doi: 10.1785/0120140240

Regional Stochastic GMPEs in Low-Seismicity Areas: Scaling and Aleatory Variability Analysis—Application to the French Alps

by Stéphane Drouet and Fabrice Cotton

Abstract We generate stochastic ground-motion prediction equations (GMPEs) for a wide magnitude range (M_w 3–8) that are adapted to the French Alps. Based on inversions of source, path, and site terms from weak-motion accelerometric data (Drouet *et al.*, 2010), we build seismological stochastic models to use in conjunction with the simulation program Stochastic-Method SIMulation (SMSIM) to stochastically simulate ground-motion response spectral amplitudes. All the input parameters are considered random variables, and the uncertainty is propagated through simulations by random sampling of the corresponding distributions. Constant and magnitude-dependent stress parameter models are compared with variable large-magnitude stress levels. Stochastic simulations are performed for periods between 0.01 and 3 s, M_w from 3 to 8, epicentral distances from 1 to 250 km, and two site conditions: rock (V_{S30} = 800 m/s) and hard rock (V_{S30} = 2000 m/s). These synthetic data are then regressed to produce stochastic GMPEs using an up-to-date regression form, the parameterization of which can be defined in terms of different distance metrics (i.e., epicentral, hypocentral, Joyner–Boore, or rupture distance). The impact of the uncertainty on each input parameter on the GMPE standard deviation is determined through sensitivity analysis. The major contributors to the uncertainty are the site model, both V_{S30} and κ (the high-frequency parameter), which affect the within-event standard deviation, and the uncertainty on the stress parameter, which affects the between-event term. The GMPEs are compared to real data using statistical analysis of residuals. Two sets of strong-motion data are considered (the Reference Database for Seismic Ground Motion in Europe [RESORCE] and the worldwide Next Generation Attenuation databases), as well as weak-motion data recorded in France. The results show that the magnitude-dependent stress parameter models (for magnitudes below 4.6) fit the French data better, and a large-magnitude constant stress parameter of 10 MPa gives a better fit to strong-motion data.

Online Material: Tables of ground-motion prediction equation coefficients.

Introduction

Because of the improvement of accelerometric networks in low-seismicity areas, moderate earthquakes (with magnitude between 3 and 5) can now routinely be recorded by regional networks. Several studies have shown however that it is not straightforward to use these new data to develop ground-motion prediction equations (GMPEs) that are reliable in the range of magnitudes and distances relevant for the seismic-hazard analysis. It has been shown that the scaling of ground motions with magnitude is magnitude dependent (e.g., Bommer *et al.*, 2007; Cotton *et al.*, 2008), and the direct extrapolation of the results of regression on data from small-to-moderate magnitude earthquakes leads to unsatisfactory predictions.

Moreover, these moderate earthquake records show regional variations of ground-motion properties (e.g., Malagnini *et al.*, 2002; Edwards *et al.*, 2008, 2011; Drouet *et al.*, 2010), which are not taken into account by classical GMPEs used for seismic-hazard assessment. Thanks to the exponential growth in the amount of data and new regression techniques, these regional variations have also been confirmed by the recent analysis of strong motions (Boore *et al.*, 2014; Stafford, 2014). To solve these issues of ground-motion scaling and regional variations, several authors (e.g., Toro *et al.*, 1997; Atkinson and Boore, 2006; Edwards and Fäh, 2013; Rietbrock *et al.*, 2013) have been developing GMPEs that are based on stochastic simulations (Boore, 2003) in which parameters are calibrated using weak-motion records. These methods have the clear advantage of taking into account a physics-based scaling of ground motion with magnitude

and the regional variations of ground-motion attenuation shown by regional records.

One of the major challenges faced by such studies is, however, the proper calibration of the simulated ground-motion variability. Indeed, the random ground-motion prediction variability associated with a given earthquake scenario (a chosen magnitude–distance pair) strongly influences the seismic-hazard computation, in particular for long-return periods (e.g., Bommer and Abrahamson, 2006). The variability of the simulation results mostly reflects the parametric intrinsic aleatory variability of the input. To our knowledge, few studies have discussed ways to calibrate the probability distributions of the stochastic model inputs, or analyzed in detail the impact of these distributions on the resulting between-event and within-event ground-motion variability.

To be of practical use, these stochastic-based GMPEs need also to fulfill several criteria. They should first be compared with the strong ground motion data from active regions. This testing step is essential to evaluate the performance of different versions of the stochastic models and, more precisely, the impact of the chosen magnitude scaling of the stress drop on the resulting ground motions. Following the suggestion of Bommer and Akkar (2012), these GMPEs should also be derived in pairs, one based on a point-source measure for use with area sources and another using an extended-source metric for fault sources.

The goal of this study is then to develop stochastic-based GMPEs in a moderate seismicity area like France. France is a country of weak-to-moderate seismicity, although analysis of historical records reveals that destructive earthquakes can strike the territory (Scotti *et al.*, 2004). Strong ground motion recordings are lacking in France. Consequently, there is no specific GMPE based on strong-motion recordings. However, for about 25 years, the national accelerometric network (Réseau Accélérométrique Permanent [RAP]) has been recording high-quality data from small events throughout France (Pequegnat *et al.*, 2008). We built a seismological model for the French Alps, and stochastic simulations are performed with Stochastic-Method SIMulation (SMSIM) (using time-domain simulation and not the random vibration theory option; see Boore, 2003). Basically, SMSIM uses a point-source model, although adjustments are included to mimic near-source and finite-fault effects. Boore (2009) compared SMSIM with actual finite-fault simulations and showed that the results are compatible when the motions are averaged over a random distribution of hypocenters. Our simulations for peak ground acceleration (PGA), peak ground velocity (PGV), and spectral accelereration from 0.01 to 3 s are performed for a wide magnitude range from 3 to 8, epicentral distances from 1 to 250 km, and two rock conditions: standard rock (V_{S30} = 800 m/s) and hard rock (V_{S30} = 2000 m/s). The simulated data are regressed to derive the stochastic GMPEs based on an up-to-date functional form.

Our approach discusses precisely the way to define region-based input parameters and capture the probability distribution of those parameters. We analyze and discuss the impact of these distributions on the resulting ground-motion variability for different frequencies and magnitude–distance pairs. All of the parameters of the seismological model are random variables, and the propagation of uncertainty in the simulations is carried out through random sampling of the input parameter distributions. A sensitivity study is performed to assess the impact of the uncertainty of each input parameter on the final GMPE uncertainty. Finally, the GMPEs are tested with real data from two international strong-motion databases (Reference Database for Seismic Ground Motion in Europe [RESORCE] and Next Generation Attenuation [NGA]) and with data recorded in France.

Seismological Model

Far-Field Fourier Amplitude Spectra

The far-field acceleration Fourier spectra can be written as a product of source, path, and site parameters (as used in Drouet *et al.*, 2010):

$$A_{ijk}(r_{ij}, f_k) = \frac{2R_{\theta\phi}}{4\pi\rho V_S^3} \times \frac{(2\pi f_k)^2 M_{0_i}}{[1 + (\frac{f_k}{f_{c_i}})^2]} \times \exp\left(-\frac{\pi r_{ij} f_k}{Q(f_k) V_S}\right) \times \frac{1}{r_{ij}^{\gamma}} \times S_j(f_k), \quad (1)$$

in which r_{ij} is the hypocentral distance from earthquake i to station j and the frequency f_k. The source is described using the usual Brune's source model (Brune, 1970, 1971) in which M_{0_i} is the seismic moment and f_{c_i} is the corner frequency of event i. Attenuation involves anelastic decay and geometrical spreading, in which $Q(f_k) = Q_0 \times f_k^{\alpha}$ is the frequency-dependent quality factor and γ is the exponent of the geometrical spreading. $S_j(f_k)$ is the site effect for station j at frequency k. V_S = 3.5 km/s is the average S-wave velocity along the path, $R_{\theta\phi}$ = 0.55 is the average radiation pattern, and ρ = 2800 kg/m^3 is the density.

This kind of very simple model has been used to analyze weak-motion events in many regions (Malagnini *et al.*, 2007; Edwards *et al.*, 2008; Drouet *et al.*, 2010) and is also used for stochastic simulations of ground motion (Boore, 2003). Still, using Brune's model, stress drop (in Pa) can be related to corner frequency and seismic moment (in N·m):

$$\Delta\sigma = \frac{7}{16} M_0 \left(\frac{f_c}{0.37 V_S}\right)^3. \quad (2)$$

In the next subsections, we will describe the seismological model used for the simulations based on the results of the Fourier spectra analysis of Drouet *et al.* (2010). Figure 1 shows the events, stations, and paths used in that study.

Stress Parameter Model

The question of the variations of the stress drop (or stress parameter as we should call it, i.e., Atkinson and Beresnev,

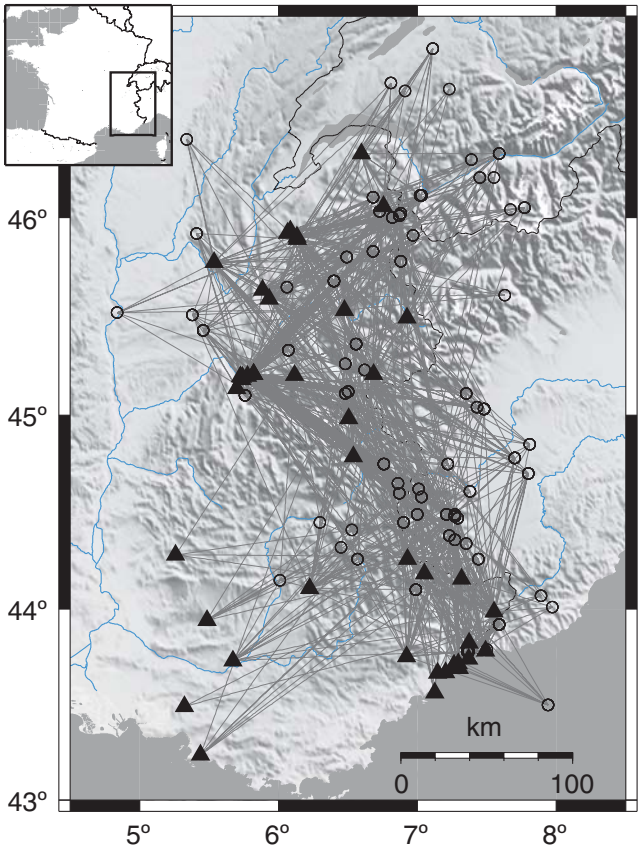

Figure 1. Map showing the earthquakes (circles), stations (triangles), and paths (gray lines) used in Drouet *et al.* (2010). The localization of the Alps region within France is also shown.

1997) with magnitude is a highly debated topic, and there are contradictory studies in the literature (see Ide *et al.*, 2003, and reference therein). Whether or not the stress drop varies with the earthquake size, a magnitude-dependent stress parameter is often needed to reproduce Fourier spectra of small-magnitude events (Edwards *et al.*, 2008; Drouet *et al.*, 2010; Edwards *et al.*, 2011).

Drouet *et al.* (2010, 2011) inverted Fourier acceleration spectra to deconvolve the source, the path, and the site terms based on data from the French metropolitan area and the French West Indies. Both datasets have been collected by the same instrumental network (the French accelerometric network, RAP) and are associated to shallow crustal earthquakes, which justify their common use to evaluate the magnitude scaling of stress drops. Figure 2 (top) shows the obtained stress drops versus magnitude for the Alps and the French West Indies. The values for the Alps present a large variability and slight variations with magnitude. However, the magnitude range is very limited. The data from the French West Indies, analyzed using the same method, span a much wider magnitude range and suggest an increasing stress drop with magnitude up to a kink point around M_w 4.6, above which the stress drop remains constant with magnitude. A very similar transition point was also suggested by data used in Edwards and Fäh (2013) and Rietbrock *et al.* (2013).

For larger magnitudes, most of the global studies of large earthquakes have shown that the stress parameter remains constant (Kanamori and Anderson, 1975; Allmann and Shearer, 2009). Allmann and Shearer (2009) demonstrated some regional variations in the stress drop, with a mean value of approximately 3 MPa for the interplate regions and 6 MPa for intraplate regions. The data obtained in the Pacific Earthquake Engineering Research–Next Generation Attenuation (PEER NGA; see Data and Resources) project give some stress-drop values for large events varying roughly between 0.1 and 10 MPa. These data are plotted in Figure 2 (bottom).

Our stress parameter model is built in the following manner. At the small-magnitude end, the model is anchored to the reference point shown in Figure 2 (top), defined as the average magnitude and average base 10 logarithm of stress drop for the Alps. At the large-magnitude end, we assume a constant stress drop and test three values: 2.5, 5, and 10 MPa. Finally, using a kink point at M_w 4.6, we draw a two-segment linear model. The three models tested for the Alps are described by equation (3) and shown in Figure 2 (bottom):

$$\ln(\Delta\sigma) = \begin{cases} a + b \times M_w, & \text{if } M_w < 4.6 \\ cste, & \text{if } M_w \geq 4.6 \end{cases} \quad \text{with } \Delta\sigma \text{ in MPa.} \tag{3}$$

The parameters a, b, and $cste$ are given in Table 1. Three other models characterized by a constant stress parameter of 2.5, 5, and 10 MPa over the entire magnitude range are also tested to allow for the possibility of self-similarity.

Regarding the standard deviation of the stress parameter, Cotton *et al.* (2013) used Brune's source model (Brune, 1970, 1971) and random vibration theory (McGuire and Hanks, 1980) to estimate the relationship between the standard deviation of stress drop and that of the PGA:

$$\sigma_{\text{stress drop}} = \frac{6}{5}\sigma_{\text{PGA}}. \tag{4}$$

Considering various empirical GMPEs, the authors estimated the standard deviations of the stress parameter to be between 0.26 and 0.59 in natural log units (between 0.11 and 0.26 in $\log_{10}$ units). They also showed that the stress parameter variability indicated in studies using spectral analysis of Fourier spectra is 3–4 times larger, which may be linked to the uncertainties in corner-frequency measurements that lead to large uncertainties in the stress parameter. Some GMPEs (e.g., Abrahamson and Silva, 2008; Chiou and Youngs, 2008) have included a variable total uncertainty with magnitude, with smaller events showing larger uncertainty. This issue is still not resolved and might simply be an effect of poor quantification of predictive variables for the small events (e.g., magnitude, distance; Bommer *et al.*, 2007) rather than reflecting a real difference in the physical process(es) between large and small events. In this study, we will assume a constant uncertainty of 0.3 in $\log_{10}$ units, which is an upper bound of the Cotton *et al.* (2013) results. As a comparison, Rietbrock *et al.* (2013) used a magnitude-dependent uncertainty for the stress

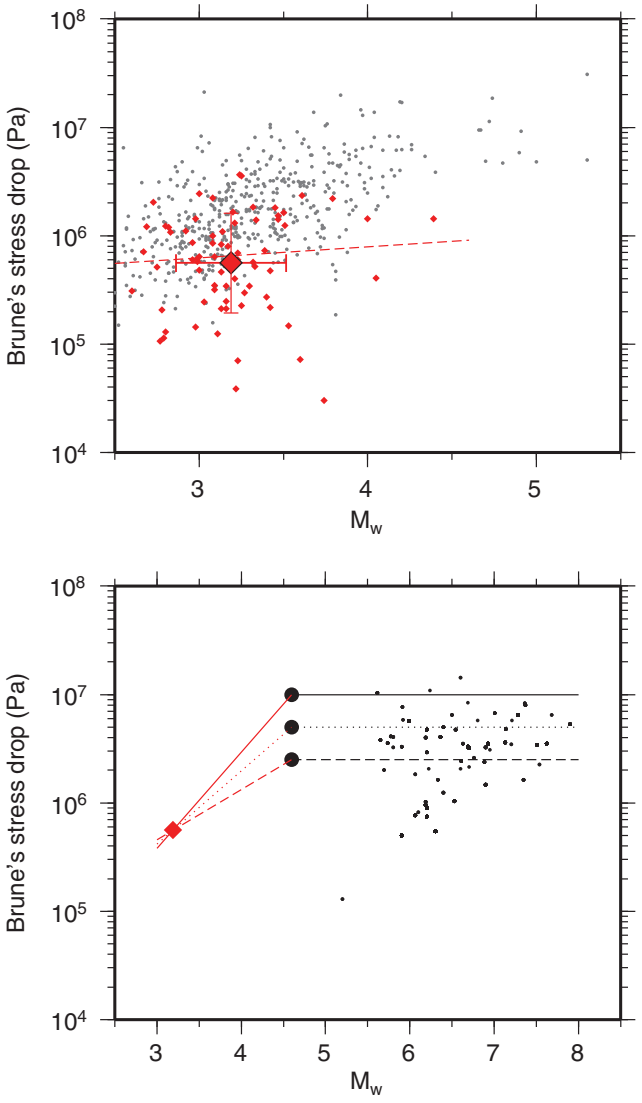

Figure 2. Top: Inverted stress drop versus moment magnitude from Drouet *et al.* (2010) and Drouet *et al.* (2011) for the Alps (red diamonds) and French West Indies (gray dots). The large square denotes the average stress drop and moment magnitude for the Alps, and the dotted line shows the scaling from the Alps data only. Bottom: Models for the stress parameter built from the average stress drop for small-magnitude events and three stress parameter values for large magnitudes (plateau at 2.5, 5, and 10 MPa). The stress drops included in the Next Generation Attenuation (NGA) database (see Data and Resources) are also indicated (dark dots).

parameter that varies between 0.3 for large-magnitude events and 0.6 for small-magnitude events.

Site Model

The site model uses the generic site amplification functions of Boore and Joyner (1997), which are parameterized in terms of V_{S30} (average shear-wave velocity over the top 30 m) as in Cotton *et al.* (2006). Two V_{S30} values are considered: 800 and 2000 m/s, because we focus on rock sites. However, as a site with the same V_{S30} can have different amplifications at different frequencies, we used various site amplification functions, scaling up and down the generic functions by a constant factor lognormally distributed. This procedure may not be very realistic because, in reality, some frequencies may be amplified and others are not, but this is an easy way to introduce some site-effect variability.

Table 1
Stress Model Parameters to Use in Equation (3)

a	*b*	*cste* (MPa)
6.7032	2.0467	10
8.2722	1.5549	5
9.8410	1.0632	2.5

The value of the standard deviation (sigma) used in this process was fixed as 0.2 in $\log_{10}$ units, based on visual comparisons with the site transfer functions from Drouet *et al.* (2010) shown in Figure 3 (top row). The gray curves are identical in the two panels and show the responses of all the stations analyzed, whereas the black curves show the stations located on rock according to two different classifications: EC8 (Eurocode 8, 2004) class A (left), and reference stations (RS) of Drouet *et al.* (2010) (right). There is very large variability in the observed amplifications, and the rock sites according to EC8 show as much variation as all the stations. It should be noted that EC8 classes for the French RAP stations are estimated using data from various approaches, and these are neither very homogeneous nor very precise (Régnier *et al.*, 2010). The RS defined as good rock sites in Drouet *et al.* (2010) show less variability.

The high-frequency attenuation parameter κ (Hanks, 1982) is determined from the Van Houtte *et al.* (2011) correlation between κ and V_{S30}. A lognormal distribution is also used to propagate uncertainties with a standard deviation of 0.2 in $\log_{10}$ units, which covers the observations from Van Houtte *et al.* (2011). For $V_{S30} = 800$ m/s, the correlation leads to $\kappa = 0.03$ s (hereafter, standard-rock conditions), and for $V_{S30} = 2000$ m/s to $\kappa = 0.01$ s (hereafter, hard-rock conditions). The resulting site amplifications and kappa values used in the simulations are shown in Figure 3.

Attenuation Model

Drouet *et al.* (2010) also computed attenuation parameters for three regions in metropolitan France, including the Alps. Their inversions provided a geometrical decay exponent, using a single segment for the whole distance range ($1/R^{\gamma}$), and a frequency-dependent quality factor ($Q(f) = Q_0 \times f^{\alpha}$). Drouet *et al.* (2010) provided some estimates of uncertainty, but only based on the *a posteriori* covariance matrix. These errors are modeling errors, are very small, and are not representative of the true observed variability.

To better define the uncertainties associated with the attenuation parameters, a bootstrap method is implemented. In this study, we randomly selected 80% of the earthquakes and 80% of the records of each of these earthquakes, and we

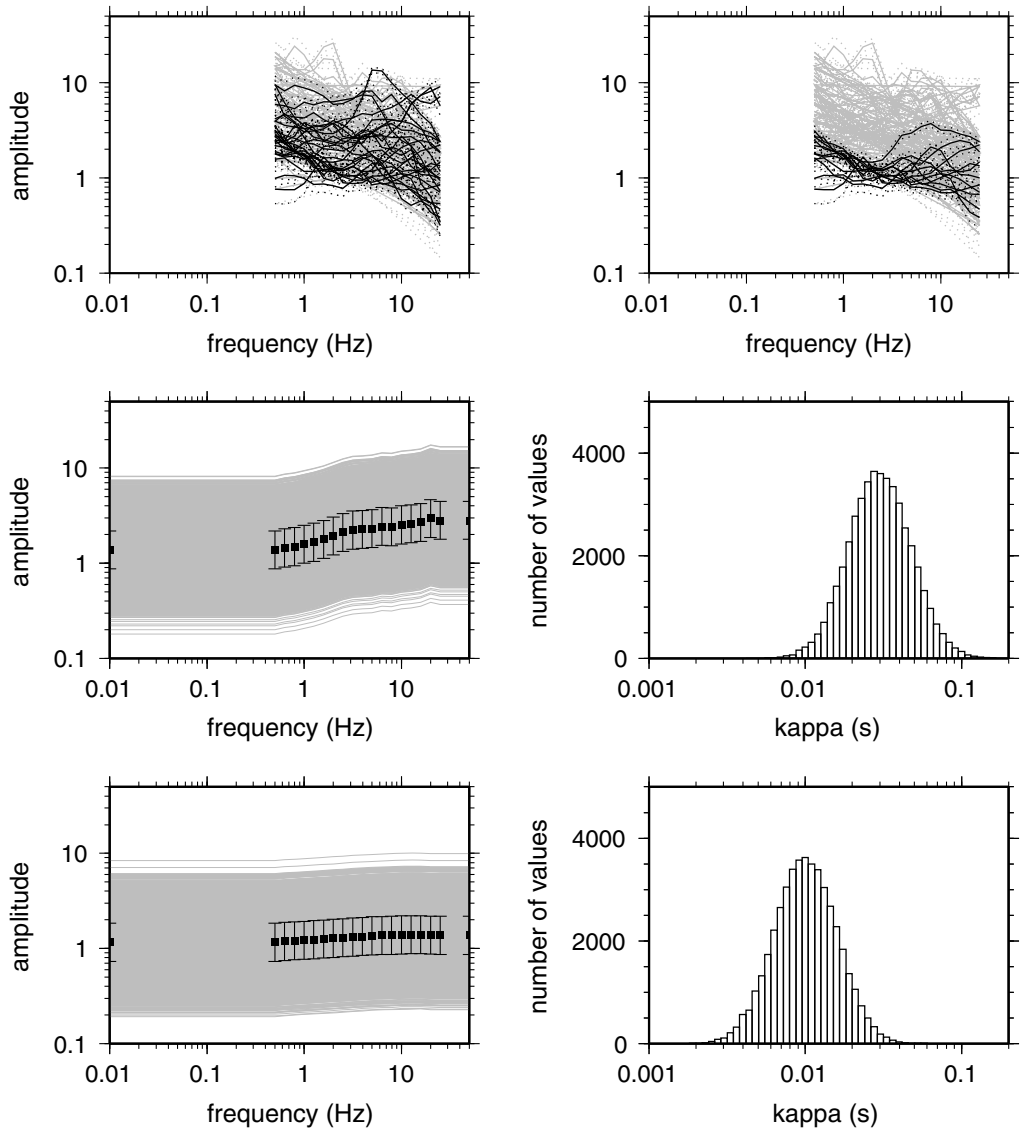

Figure 3. (Top row) Site amplification curves for the Réseau Accélérométrique Permanent (RAP) stations, as given in Drouet *et al.* (2010) (gray curves). EC8 class A stations (top left) and reference stations selected in Drouet *et al.* (2010) (top right) for the Alps are indicated (black curves). (Middle and bottom row) Site models used in the simulations for a standard rock site $V_{S30} = 800$ m/s, $\kappa = 0.03$ s (middle) and a hard rock site $V_{S30} = 2000$ m/s, $\kappa = 0.01$ s (bottom), for the generic amplification (left: gray curves are the individual models, black squares and lines show the median and median $\pm\sigma$ amplifications, respectively), and the distribution of the κ values (right).

duplicated some of the data to keep almost the same amount of total data compared to the original dataset. This operation is done 100 times, and for each dataset we ran the inversion method of Drouet *et al.* (2010).

In this way, we end up with 100 sets of parameters, from which we can draw distributions that represent the observed variability (Fig. 4). It can be noted that the distributions can be fitted by normal distributions. The attenuation parameters determined with the bootstrap technique are given in Table 2. The median values of the parameters are very close to those from Drouet *et al.* (2010), but the standard deviations from the bootstrap analysis are much larger here and are assumed to better represent the true variability. Formally, the parameters are not independent and correlations should be taken into account for the analysis of the standard deviations; however, for the sake of simplicity and to remain conservative, we assume independent attenuation parameters.

Duration Model

The last parameter needed for the simulations of ground motion is the path duration function. The total duration results from the combination of the source duration, assumed to be the reciprocal of the source-corner frequency (Boore, 2003), the effect of path propagation and scattering, and other effects linked with the site condition or complex source effects such as directivity (Kempton and Stewart, 2006).

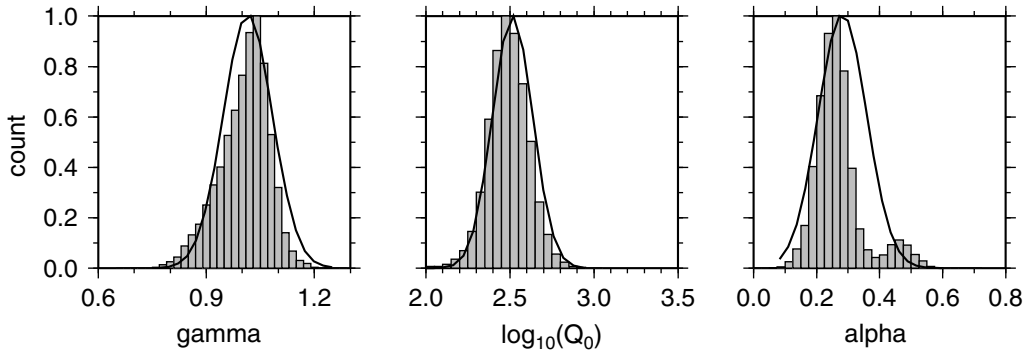

Figure 4. Distributions for the attenuation parameters for the Alps, after applying the bootstrapping method to the results of Drouet *et al.* (2010) and associated Gaussian models: (left) γ; (middle) $\log_{10}(Q_0)$; (right) α.

Various definitions of duration exist (Bommer and Martínez-Pereira, 1999), but one category is widely used: the significant duration is defined as the time interval across which a specified amount of energy is dissipated. Energy can be represented as the integral of the squared velocity or acceleration, and usually one selects duration as the interval including 5%–75% or 5%–95% of the total energy. Edwards and Fäh (2013) and Bora *et al.* (2014) showed that the duration of the stochastically simulated data using SMSIM lies between the two measures defined above.

Duration of ground motion was not studied in Drouet *et al.* (2010). Consequently, we computed duration using exactly the same dataset, from both velocity and acceleration data, and using the two criteria 5%–75% and 5%–95% of the energy. We computed the integrals of the squared acceleration and velocity within a time window defined by the *S*-wave onset and the *S*-wave onset plus 50 s. We limited the integration to 50 s due to the heterogeneity of the total length of the time series within the dataset, and we used only *S* waves to be consistent with SMSIM, which simulates *S* waves. We subtracted the source duration (computed as $1/f_c$, in which f_c is the source-corner frequency as given in Drouet *et al.*, 2010, for each event) from the total duration to estimate the path duration, which is the required parameter for the stochastic simulation program SMSIM.

Figure 5 shows the computed path durations based on the two energy criteria and using both velocity and acceleration. Obviously path durations computed from the 5%–75% criteria are shorter than those based on the 5%–95% criteria. One can also observe that acceleration and velocity lead to very similar results. Figure 5 shows that as a first approximation, a two-segment linear model fits fairly well the average data per distance bins, with a kink point at 70 km for the 5%–75% energy model and at 60 km for the 5%–95% energy model. We tried to identify any dependence on site conditions, but due to the large dispersion and poor characterization of the French accelerometric stations, the tests were not conclusive. Consequently, we used all the data to build the path duration model, although we are interested in simulations for rock sites.

Table 2
Attenuation Model Parameters

γ	$\log_{10}(Q_0)$	α
1.04 ± 0.07	2.52 ± 0.12	0.28 ± 0.08

To check the consistency between the input duration model and the output durations computed from the stochastically simulated time series, we ran a number of simulations for various magnitude and distance combinations (see the Simulation Settings section for details on the simulation settings). The propagation of uncertainty on the duration is carried out using a uniform distribution on the duration value at the kink point as well as on the slope of the second segment. Figure 6 compares the input ($T_{\text{path}}^{\text{input}}$) and output ($T_{\text{path}}^{\text{output}}$, computed on the simulated acceleration time series) path durations. It shows that $T_{\text{path}}^{\text{output}}$ computed from the 5%–95% energy criteria are close to the input durations. However, the output durations are systematically smaller than the input durations and the greater the magnitude, the larger the difference. Using only the small magnitudes, to be consistent with our input real data, we found a relationship: $T_{\text{path}}^{\text{output}} = 0.95 \times T_{\text{path}}^{\text{input}}$. The same results were found by Edwards and Fäh (2013), but they did not notice any magnitude dependence, and they adjusted their input path duration model to account for those differences (about 8%). Here, we also adjust our input model, based on the 5%–95% criteria, up by 1.05.

The final duration model can be written as

$$T_p = \begin{cases} R_h \times 18.20/60, & \text{if } R_h < 60 \text{ km} \\ 18.2 + 0.05 \times (R_h - 60), & \text{if } R_h \geq 60 \text{ km} \end{cases}. \quad (5)$$

We modeled uncertainties using uniform distributions for the duration at the kink point, with a standard deviation of 8 s, and on the slope of the last segment, using a standard deviation of half its value, consistent with the observations in Figure 5.

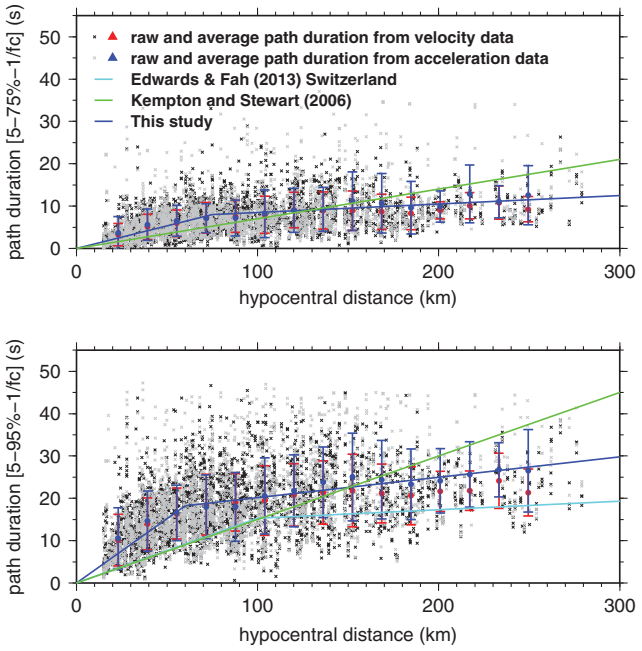

Figure 5. Path duration computed using the dataset for the Alps of Drouet *et al.* (2010) as a function of the hypocentral distance using (top) the 5%–75% energy criteria and (bottom) the 5%–95% energy criteria. Raw data and average values for a number of distance bins are shown for both velocity data and acceleration data. The two-segment linear fit to the data (blue line) is compared with the models of Edwards and Fäh (2013) for Switzerland and Kempton and Stewart (2006) worlwide.

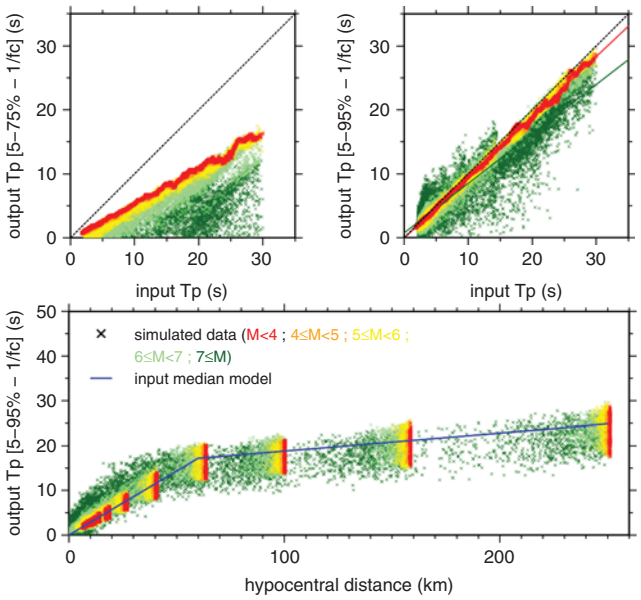

Figure 6. Comparison of input path duration and output path duration computed from the total duration (5%–95% of the energy) minus the source duration computed as $1/f_c$ (left). Output path duration versus hypocentral distance compared with the average input model.

Simulations and GMPEs

Simulation Settings

Simulations are performed for moment magnitudes from 3 to 8, using 0.5 unit steps. For each magnitude, a random fault orientation is defined (i.e., strike and dip, with the dip constrained to be greater than 10°). A fictitious focal mechanism is assigned based on the dip angle (reverse mechanism for a dip lower than 40°, strike-slip mechanism for a dip greater than 75°, and normal mechanism otherwise). There is no clear evidence of predominant focal mechanisms in the Alps region as defined here, except maybe a predominant extensional regime in the inner Alps (Sue *et al.*, 1999). However, because we do not intend to include the focal mechanism as a predictor variable, and because the fault orientation is only used for computing fault dimensions (see below) and the various distance metrics, we use a uniform distribution for the dip angle.

The hypocentral depth is estimated based on the updated earthquake catalog for France (Cara *et al.*, 2015). The depth distribution for the Alps has a peak around 7 km, a couple of events with negative depth and tend to 0.0 below 20 km. Considering the large errors in the depth distribution, we choose to define a distribution with a plateau between 5 and 10 km, and cosine tapers between 2 and 5 km, as well as between 10 and 13 km.

Fault dimensions (length and width) are estimated from the Wells and Coppersmith (1994) relationships:

$$\log_{10}(W) = \begin{cases} -0.76 + 0.27 \times M_w & \text{for strike-slip events} \\ -1.14 + 0.35 \times M_w & \text{for normal-faulting events} \\ -1.61 + 0.41 \times M_w & \text{for reverse-faulting events} \end{cases} \quad (6)$$

and

$$\log_{10}(L) = \begin{cases} -2.57 + 0.62 \times M_w & \text{for strike-slip events} \\ -1.88 + 0.50 \times M_w & \text{for normal-faulting events} \\ -2.42 + 0.58 \times M_w & \text{for reverse-faulting events} \end{cases}, \quad (7)$$

in which L is the subsurface fault length in kilometers, and W is the subsurface fault width in kilometers. To include additional variability in the fault dimensions, for each simulation, the input moment magnitude used in the above equations is modified randomly using a normal distribution with standard deviation 0.3. This procedure allow us to simulate fault planes of different dimensions for the same magnitude. The Wells and Coppersmith (1994) relationships are extrapolated beyond their validity range, especially for small magnitudes. This does not have a strong influence on the simulations due to the very small fault extension for small magnitude and because the fault extension is only used to compute the different distance metrics.

Forty different mechanisms are simulated for each moment magnitude. Figure 7 shows the fault length and width

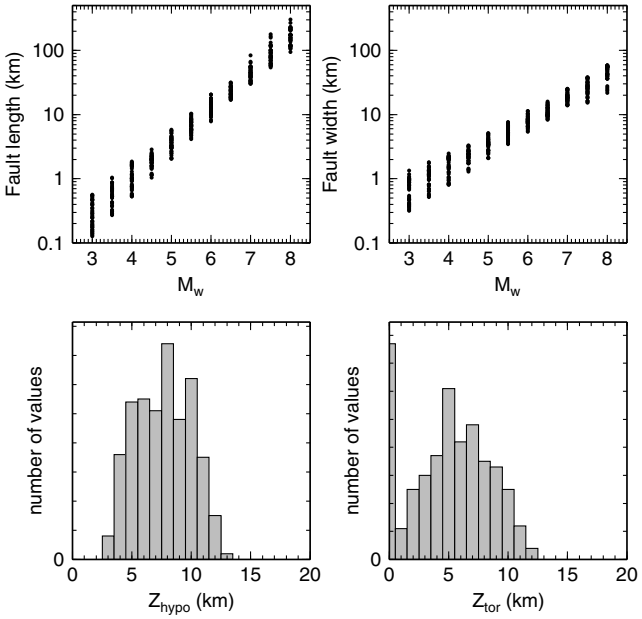

Figure 7. (Top left) Fault length and (top right) width computed using Wells and Coppersmith (1994) relationships for each magnitude sampled. The relationships are extrapolated beyond their validity range. (Bottom left) The focal depth and (bottom right) depth to top-of-rupture for the simulated dataset.

versus magnitude for all the simulated events, as well as the distributions of the focal depths and the depths to the top-of-rupture. For a given mechanism, epicentral distances from 1 to 250 km and source-to-site azimuths from 0° to 360° are simulated. Given the synthetic fault parameters and a randomly chosen hypocenter position on the fault, three other types of distances commonly used in GMPEs are computed: the Joyner–Boore distance (R_{JB}; closest horizontal distance to the surface projection of the fault plane), the rupture distance (R_{rup}; closest distance to the fault plane), and the hypocentral distance (R_{hyp}). Kaklamanos *et al.* (2010) developed a computation scheme to compute R_{rup} from R_{JB}. We slightly modified the Kaklamanos *et al.* (2010) relationships to compute (from geometrical considerations) all of the distance types based on the epicentral distance and on the source-to-site azimuth. The distances metrics are compared in Figure 8, which shows that, as expected, R_{epi} is always greater than or equal to R_{JB}, and R_{hypo} is always greater than or equal to R_{rup}.

Figure 9 shows the simulated spectral accelerations at 0.01 s for the Alps (using the variable stress model with a plateau value of 10 MPa and for standard-rock conditions) versus the Joyner–Boore and rupture distances and for M_w 4.5 and 6.0. The medians of some recent GMPEs are compared to the stochastic data. Models for Europe and the Middle East are selected: the Akkar and Bommer (2010) model (herefater, AB10) and the Bommer *et al.* (2007) model (hereafter, B2007), which is based on the same functional form and data as the previous one but also includes small-magnitude data. Worldwide models for active regions are also selected: the Boore and Atkinson (2008) (hereafter BA2008) and Chiou and Youngs

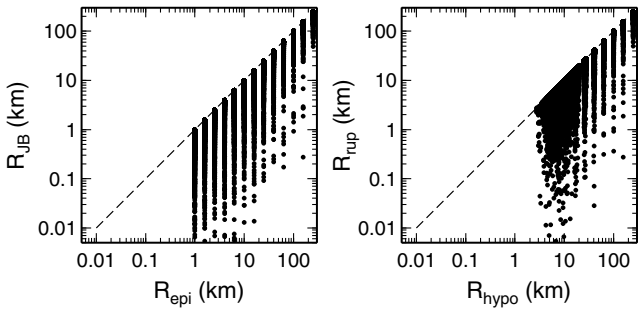

Figure 8. Comparison between (left) epicentral and Joyner–Boore distances and (right) hypocentral and rupture distance for the simulated dataset.

(2008) (hereafter CY2008) models (mainly for California and Taiwan) and the Cauzzi and Faccioli (2008) model (hereafter CF2008). We also include one model for a stable continental region: the Atkinson and Boore (2006) model (hereafter AB2006) for eastern North America. Modifications of some of these GMPEs exist to account for small-magnitude data. Atkinson and Boore (2011) adjusted BA2008 and AB2006 (hereafter BA2008 modif. 2011 and AB2006 modif. 2011, respectively) and Chiou *et al.* (2010) adjusted CY2008, including data from two Californian subregions (hereafter CY2008 modif. 2010). The AB10 model implemented here includes the high-frequency extension of Bommer *et al.* (2012). The parameters for each GMPE are chosen to reflect the standard-rock conditions. Figure 9 shows that the simulated median amplitudes are consistent with those predicted from empirical models for small and moderate magnitudes.

Regression Analysis

Stochastic GMPEs are built from the stochastically simulated data using regression analysis, as is done for the analysis of real data. The functional form adopted is the following:

$$\ln(y) = b_1 + b_2 \times (M_w - 8) + b_3 \times (M_w - 8)^2 + (b_4 + b_5 \times M_w) \times \ln\left(\sqrt{R^2 + b_6^2}\right) + b_7 \times R, \quad (8)$$

in which y is the ground motion in meters per second squared; R is either the epicentral, the hypocentral, the Joyner–Boore, or the rupture distance; and the coefficients b_1 to b_7 are obtained from the regression. The adopted functional form takes into account a squared-magnitude term (Fukushima, 1996; Douglas and Jousset, 2011) and magnitude-dependent distance scaling (Bommer *et al.*, 2007; Cotton *et al.*, 2008).

Two regression techniques were compared: standard least-squares (LS) and random-effect maximum-likelihood (ML) regressions. The main advantage of the second technique is to take into account systematic differences between events through partitioning the residuals (Abrahamson and Youngs, 1992; Stafford, 2014). Given the roughly even distribution of the simulated data in terms of magnitude and distance, the two methods lead to the same results. However, the ML method is preferred because it gives the within-event

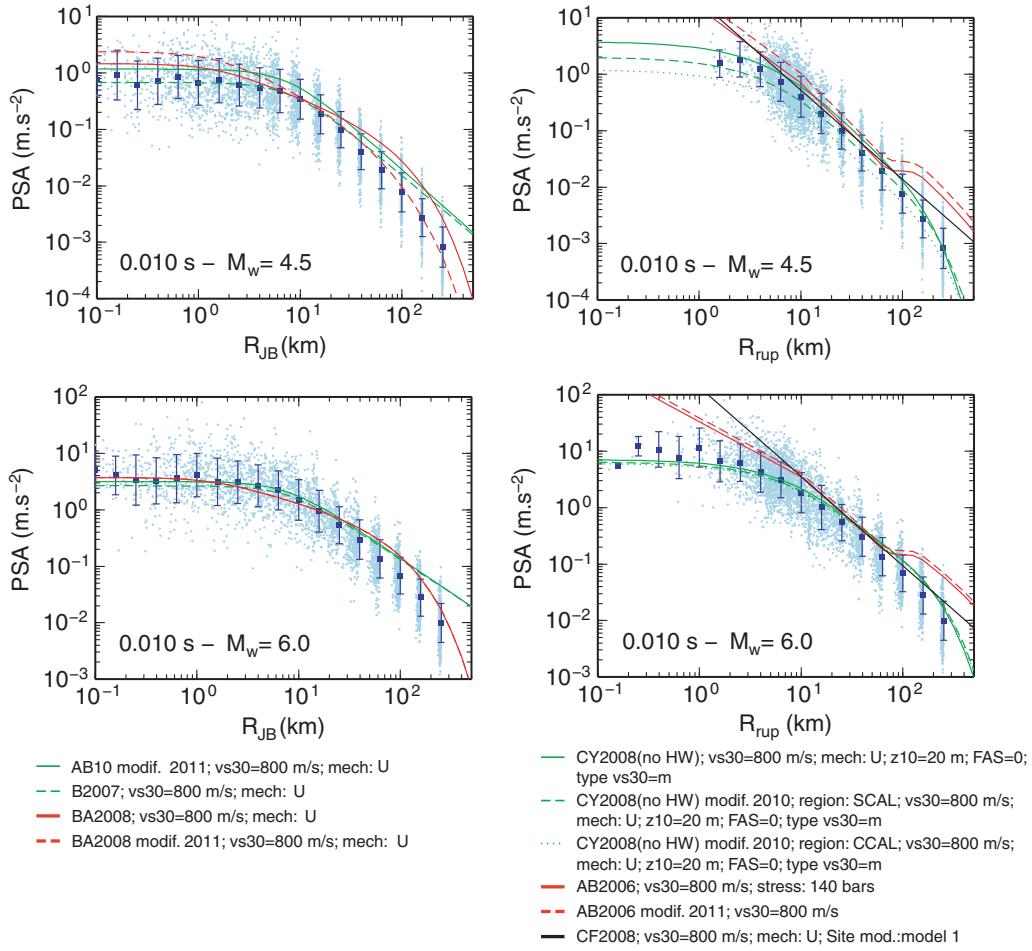

Figure 9. Stochastically simulated pseudospectral acceleration (PSA) (0.01 s) for the Alps (blue dots, raw data; squares and error bars, average data) using the variable stress model with plateau at 10 MPa. Data are shown versus (left) Joyner–Boore distance and (right) rupture distance for (top) M_w 4.5 and (bottom) M_w 6. See text for the ground-motion prediction equations (GMPEs) codes definitions.

and between-event uncertainties. To achieve rapid convergence of the ML method, we use the preliminary results of the LS method as the input for the ML method.

Some tests were also performed regarding the functional form; the "−8" in the magnitude terms only helps to have absolute values of the coefficients that are more homogeneous between the different terms (other values could have been chosen). The b_6 term (pseudodepth) appears to be necessary to account for the near-source saturation that is included in the simulations, even for distance metrics that already take into account some depth information. However, the absolute value of b_6 is smaller when the hypocentral distance is used, followed by the rupture distance, and then by the Joyner–Boore and epicentral distances, all of the other coefficients being similar.

Figure 10 compares the various versions of the stochastic GMPEs for the Alps: the variable stress parameter models (with plateau values of 2.5, 5, and 10 MPa), the constant stress parameter models (5 MPa for all magnitudes) for standard-rock sites, and the variable stress parameter model (plateau value of 5 MPa) for hard-rock sites. For large magnitudes, the variations linked with the large-magnitude stress parameter values are obvious, as is the similarity of the constant and variable stress model (i.e., the variable stress models are only variable for small magnitudes). In contrast, for small magnitudes (M_w 3), the three variable stress parameter models are similar and the constant stress parameter model leads to higher values. These results are clearly expected from the input stress parameter model (see Fig. 2). The differences are more pronounced for short periods than for long periods. The hard-rock site model leads to slightly higher and lower amplitudes at short and long periods, respectively, compared to the rock model for the same parameters (i.e., variable stress parameter with a large-magnitude value of 5 MPa). One important difference concerns the standard deviation, which is reduced and is shifted to a lower period peak for the very-hard-rock model compared to the rock model.

Sensitivity Analysis

All the input parameters are described by distributions, and the uncertainties on these input parameters are propagated through the simulations using random sampling of the distributions. One very important piece of information

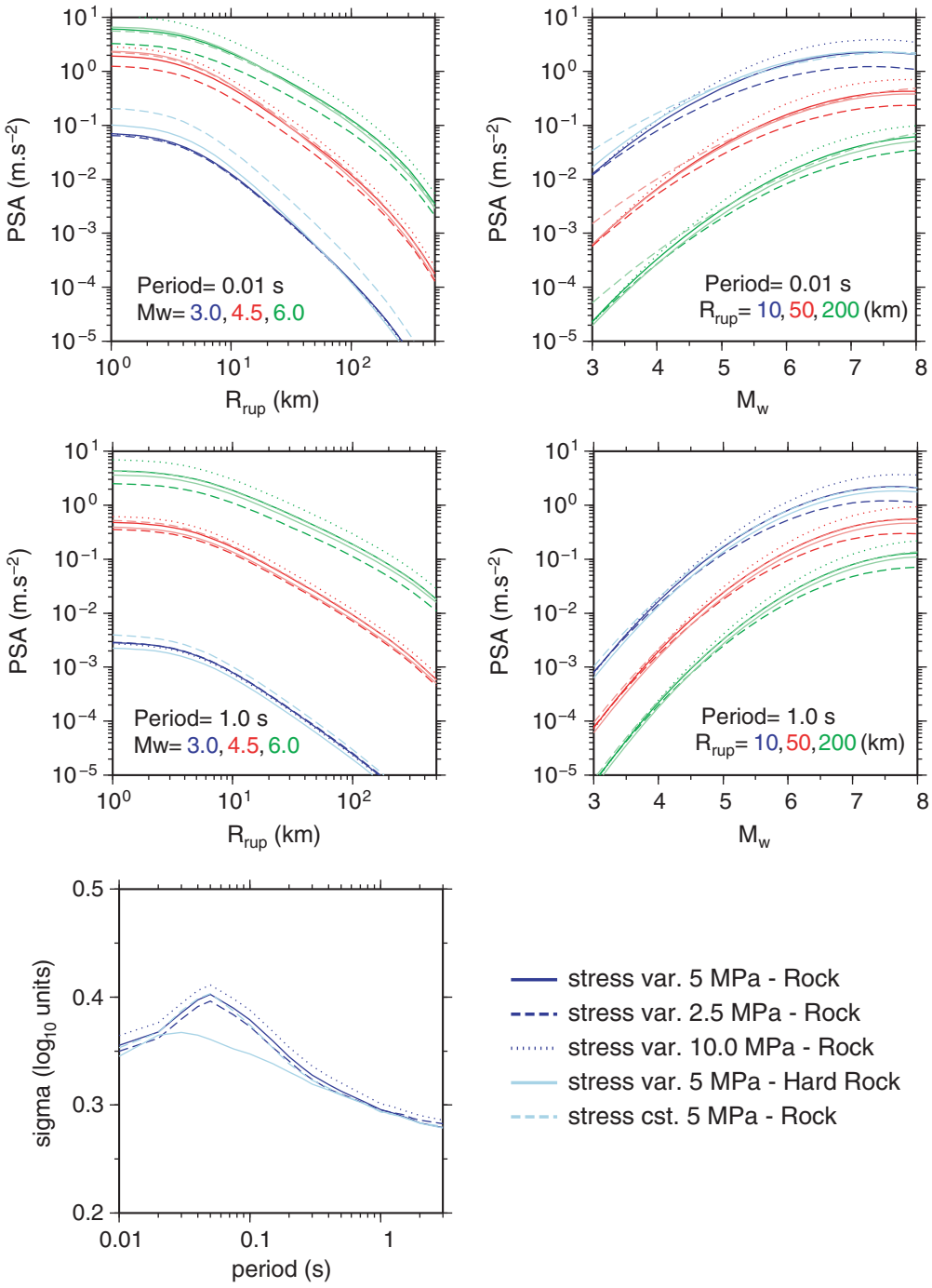

Figure 10. Comparison of the different versions of the stochastic ground-motion prediction equations (GMPEs): amplitude versus (left) distance and (right) magnitude, for (top) PSA (0.01 s) and (middle) PSA (1.0 s). The total standard deviations are also shown (bottom left).

is how these uncertainties affect the final GMPE uncertainty. Consequently, a set of nine GMPEs were computed, taking into account the uncertainty on each parameter, one by one (all of the others set to their median values):

1. SMSIM uncertainty: vertical faults with fixed strike (north), hypocenter located at 50% of the fault length and 70% of the fault width;
2. uncertainty on duration;
3. uncertainty on the fault plane: random orientation and random hypocenter position;
4. uncertainty on anelastic attenuation: Q_0 and α;
5. uncertainty on geometric attenuation;
6. uncertainty on κ;
7. uncertainty on site amplification;
8. uncertainty on stress parameter; and
9. all uncertainties.

The coefficients determined with each of these models are almost identical. However, the standard deviations vary a lot

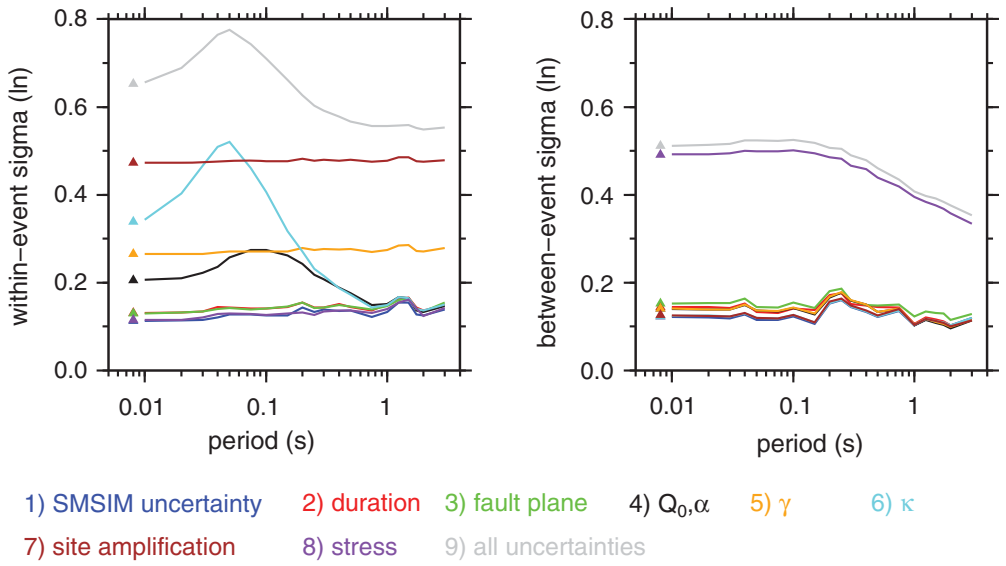

Figure 11. (Left) Within-event and (right) between-event uncertainties obtained for the nine models used in the sensitivity analysis.

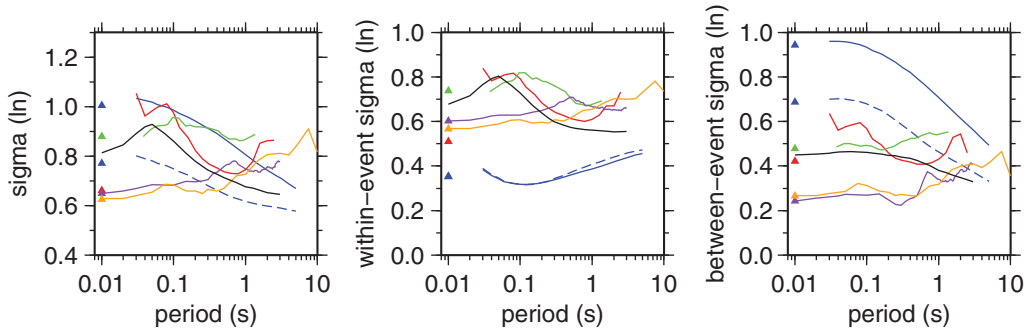

Figure 12. Comparison of (left) total, (middle) within-event, and (right) between-event standard deviations for the Alps stochastic GMPEs and other published GMPEs: Akkar and Bommer (2010) (purple), Boore and Atkinson (2008) (orange), Edwards and Fäh (2013) (red), Rietbrock *et al.* (2013) constant and variable stress parameter model (solid and dashed blue, respectively), Rodriguez-Marek *et al.* (2011) (green).

depending on the model (Fig. 11). The major contributions to the total uncertainty come from the site amplification and κ (which affect the within-event term, i.e., the record-to-record variability) and from the stress parameter (which affects the between-event term, i.e., the event-to-event variability). The shape of the within-event term is mainly controlled by κ. The uncertainty of κ introduces a peak centered at a period of around 0.05 s and influences periods from 0.01 to about 0.2–0.3 s. For long periods (> 1 s), its influence is negligible. The results using hard-rock site conditions show that the amplitude and the dominant period of this peak decrease (see Fig. 10, bottom left). The between-event term, controlled by the stress parameter uncertainty, also varies with period, with a slow decrease for periods above 0.1–0.2 s, although it remains a large contributor to the total uncertainty for all of the periods. The attenuation parameters also influence the within-event term. The influence of the anelastic attenuation parameter uncertainty varies with the period and shows a peak around 0.1 s, where its influence is as large as that of γ. At smaller and larger periods, its influence decreases and becomes negligible for long periods (> 1 s). The influence of γ remains constant for all periods. Comparatively, the uncertainties linked with the duration, the fault-plane orientation, and the hypocenter location on the faults have very little impact on the total GMPE uncertainty.

Figure 12 compares the standard deviations for various GMPEs (empirical for active regions, Europe and Japan, and stochastic for the United Kingdom and Switzerland) and shows that the spread is considerable from 0.6 to 1.0 in natural logarithm units. The shapes of the curves are also highly variable. Most of the models show large standard deviations at short periods, except for the Akkar and Bommer (2010) and Boore and Atkinson (2008) models, which show increases at long periods. It can be noted that the Boore and Atkinson (2008) GMPE compared to the other NGA models has a low-reported standard deviation and can be seen as a lower bound for the NGA models set.

Figure 12 shows that, excluding the Rietbrock *et al.* (2013) model, the within-event sigma appears slightly less variable than the total sigma. The Rietbrock *et al.* (2013) model

does not consider variability for the site conditions, which explains the very low within-event sigma. The peak in the within-event sigma is located between 0.04 s and 0.08 s for the Edwards and Fäh (2013) model, as well as for the model presented in this study. Both models use similar rock reference conditions and comparable κ. On the other hand, the Rietbrock *et al.* (2013) model uses very hard-rock reference conditions and might have a peak below 0.03 s, which is confirmed by our tests using the very hard-rock site conditions, but which does not appear clearly in Figure 12 due to the missing data at short periods for Rietbrock *et al.* (2013).

Looking at the empirical GMPEs, the Rodriguez-Marek *et al.* (2011) model has the same kind of shape, with decreasing sigma with period, and a wide peak extending from about 0.04 s to 0.3 s. They used a dataset from Japan that was characterized by a V_{S30} distribution that ranged from 200 to 1000 m/s, with a peak at 500 m/s (Rodriguez-Marek *et al.*, 2011). Consequently, their site reference condition is close to soft-rock sites. Regarding the Boore and Atkinson (2008) and Akkar and Bommer (2010) models, there is no visible peak in the within-event terms, and their shapes are also different. One explanation might be that these models include data that cover a wide range of site conditions, as well as events from various regions, which can cause variations in attenuation characteristics. Chiou *et al.* (2008) presented the NGA database, and the V_{S30} distribution shows that most stations have V_{S30} lower than 500 m/s, with a peak around 200 m/s. Akkar and Bommer (2007) reported the proportions of the rock (National Earthquake Hazards Reduction Program [NEHRP] class A and B) as stiff, soft, and very soft site conditions, which were 33%, 41%, 24%, and 2%, respectively; this classification was used in Akkar and Bommer (2010). However, there is still a 0.1–0.2 difference in the within-event term from these models compared to the others.

Regarding the between-event sigma, the models that include small-magnitude events (Rodriguez-Marek *et al.*, 2011; Edwards and Fäh, 2013; Rietbrock *et al.*, 2013) have higher between-event sigmas (approximately 0.5) than the models that include mostly events with $M_w > 5$ (Boore and Atkinson, 2008; Akkar and Bommer, 2010), which lead to between-event sigmas of approximately 0.3. This difference decreases for periods greater than approximately 2 s. The Rietbrock *et al.* (2013) models, which use large uncertainty on the stress parameter (from 0.3 up to 0.6, depending on magnitude), present very high between-event sigmas. The shape and the low-period level of the between-event sigma is controlled by the uncertainty of the stress parameter.

Comparison with Real Data

The residuals between observed and predicted spectral ground-motion amplitudes are analyzed here using the methods described in Scherbaum *et al.* (2004, 2009). Normalized residuals with respect to a given GMPE are computed as shown in equation (4):

$$\text{res} = \frac{\log_{10}(y_{\text{obs}}) - \mu}{\sigma}, \tag{9}$$

in which μ and σ are the median and standard deviation of the logarithm of the ground motion predicted by the GMPE, and y_{obs} is the observed ground-motion value. The mean, median, and standard deviations of the distribution of the normalized residuals are computed as well as the median of the likelihood (LH) distribution, and the combination of this information can be used to rank (in a subjective way) the ability of the GMPE to fit the data distribution (Scherbaum *et al.*, 2004). Also, the log-likelihood (LLH) criterion (see Scherbaum *et al.*, 2009) is estimated, which is a measure of the quality of the fit, or more precisely, a measure of the relative distance between the GMPEs and the data.

Large-Magnitude Data

One of the questions is how to choose the large-magnitude stress parameter, which can take on three different values (2.5, 5.0, and 10 MPa). To quantify the fit between these models and the real data, we used two recent databases of strong ground motions: the RESORCE database (Akkar *et al.*, 2014), which was built in the context of the SeIsmic Ground-Motion Assessment (SIGMA), and the PEER NGA database, which includes recordings from many active regions around the world (Chiou *et al.*, 2008).

Only data corresponding to $M_w \geq 5$ (in order to sample the constant stress part of our models which starts at M_w 4.6) and to $V_{S30} \geq 750$ m/s (to be consistent with the definition of our models for rock sites) are used. After the selection, data from M_w 5–7.6, and R_{JB} = 0–278 km (R_{rup} = 2–279 km) from RESORCE, and M_w = 5.2–7.9 and R_{JB} = 0–152 km (R_{rup} = 2–152 km) from NGA, were kept. Here, 18 periods between 0.01 and 3 s were used, as well as PGA and PGV, which resulted in a total of 513 and 1420 data points for RESORCE and NGA, respectively.

The results of the residuals analysis are shown in Table 3. There is generally good agreement between the models and the data, as good ranking scores are achieved (A or B, see Scherbaum *et al.*, 2004, for the definition of the ranks) and the LLH are relatively small. Beauval *et al.* (2012) quantified the interval of variation of the LLH using synthetic tests. They showed, based on synthetic data, that an LLH of approximately 1.5–1.6 indicates an almost perfect fit, whereas for values > 3–4, the normalized residual distribution, which for a perfect fit would be Gaussian with zero mean and unitary standard deviation (a standard Gaussian distribution), moves away from the standard Gaussian distribution. In real applications, an LLH value below 2.5 indicates a reasonable fit.

For the RESORCE and the NGA data, the model using a stress parameter of 10 MPa leads to a better fit than the other two options. It is interesting to note that using the 5 MPa model, the mean and median of the residuals distributions are positive, whereas they turn negative with the 10 MPa model. For the NGA data, they are only slightly negative. This result suggests that an intermediate stress parameter

Table 3

Results of the Comparison between the Real Data from the Reference Database for Seismic Ground Motion in Europe (RESORCE) and Next Generation Attenuation (NGA) Databases and the Stochastic Ground-Motion Prediction Equations (GMPEs)

Data	Large-Magnitude Stress Parameter	Distance Metric	Mean NR (rank)*	Median NR (rank)*	Std NR (rank)*	Median LH (rank)*	Rank*	LLH
RESORCE data	Stress 10 MPa	R_{rup}	−0.134 (A)	−0.208 (A)	1.029 (A)	0.512 (A)	A	2.101
	Stress 5 MPa	R_{rup}	0.357 (B)	0.303 (B)	1.048 (A)	0.514 (A)	B	2.208
		R_{JB}	0.334 (B)	0.285 (B)	0.958 (A)	0.542 (A)	B	2.067
		R_{hypo}	0.347 (B)	0.303 (B)	0.976 (A)	0.540 (A)	B	2.098
		R_{epi}	0.266 (B)	0.234 (A)	0.943 (A)	0.548 (A)	B	2.017
	Stress 2.5 MPa	R_{rup}	0.918 (D)	0.870 (D)	1.057 (A)	0.350 (B)	D	2.739
NGA data	Stress 10 MPa	R_{rup}	−0.071 (A)	−0.027 (A)	0.858 (A)	0.585 (A)	A	1.860
	Stress 5 MPa	R_{rup}	0.522 (C)	0.559 (C)	0.883 (A)	0.467 (A)	C	2.084
		R_{JB}	0.521 (C)	0.558 (C)	0.865 (A)	0.472 (A)	C	2.061
		R_{hypo}	0.779 (D)	0.786 (D)	0.955 (A)	0.388 (B)	D	2.422
		R_{epi}	0.357 (B)	0.303 (B)	1.048 (A)	0.514 (A)	B	2.208
	Stress 2.5 MPa	R_{rup}	1.212 (D)	1.261 (D)	0.904 (A)	0.204 (C)	D	2.974

NR, normalized residuals; LH, likelihood; LLH, log likelihood.
*The ranking categories are those defined in Scherbaum *et al.* (2004).

value may perform even better. One can also note that the ranking and the LLH values vary depending on the distance metrics used, but we could not determine any systematic trend. This may strongly depend on the quality of the finite-fault information for the real data. It is also interesting to note that the standard deviations of the normalized residual distributions are close to 1, which indicates that the GMPE standard deviations are consistent with the real data dispersion. In turn, it shows that the uncertainties on the input parameters were well calibrated.

Low-Magnitude Data

In this section, we use the data recorded by the RAP in the Alps regions (Drouet *et al.*, 2010). For this data, the site conditions are not known with precision, information is heterogeneous, and only a couple of V_{S30} are available with precision. Régnier *et al.* (2010) made a big effort to compile the available data and to classify the stations according to the EC8 classes (Eurocode 8, 2004). Two other classifications are considered in this study: one is based on the inverted site transfer functions of Drouet *et al.* (2010) (stations showing amplifications <2 over the whole frequency band are classified as rock sites; flat response [FR] condition); and the other uses the reference sites chosen in the inversions presented in Drouet *et al.* (2010), which are assumed to be the best rock sites in the dataset (RS condition). Table 4 shows that the magnitudes and the distance ranges remain similar regardless of the site classification, although the amount of data available varies considerably.

Table 4

Parameters of the Dataset for France for the Different Site Classification Schemes

Site Classification	$R_{rup_{min}}$	$R_{rup_{max}}$	$M_{w_{min}}$	$M_{w_{max}}$	Ndata*
EC8	17	329	2.6	4.4	7625
Flat response	21	251	2.6	4.4	1932
Reference stations	19	251	2.6	4.4	4514

*From 20 periods between 0.01 and 3 s.

Table 5 shows the results of the residuals analysis for the Alps. Both types of models, with variable or constant stress parameter, were tested. For each type, three plateau values were considered: 2.5, 5, and 10 MPa (see Fig. 2). Testing is also performed for the different site classifications (EC8, FR, and RS). The results vary depending on the site condition used, but one can note that a better fit is achieved with the variable stress models (regardless of the large-magnitude plateau) or with the constant stress model at 2.5 MPa; the lowest LLH values are obtained in those cases. The constant stress models using 5 or 10 MPa overpredict the data as can be seen by the large means and medians of the residuals distributions. This was expected because the inverted stress parameters for the small events in the Alps are low (see Fig. 2). The results using the EC8 classification always lead to a poorer fit than the other two classifications. As shown in Figure 3, the stations classified as EC8 rock sites present a very large variability. We believe that the other two classifications are more representative of rock sites. The RS condition should even be closer to hard-rock site conditions. Consequently, we also tested the hard-rock version of the stochastic GMPEs (Table 5), but the results are similar to those obtained with the standard-rock model. Using different distance metrics does not impact the results much, which was expected, due to the small fault extension for weak-motion data. Figure 13 compares the variable stress parameter model (large-magnitude level 10 MPa) with recorded rock data for period 0.01 s. Both distance and magnitude scaling are well reproduced.

Comparison with Other European Stochastic Models

Two stochastic models have been recently developed for the United Kingdom (Rietbrock *et al.*, 2013) and for Switzerland (Edwards and Fäh, 2013; Cauzzi *et al.*, 2015). Rietbrock

Table 5
Results of the Comparisons between the Real Data Recorded in the Alps and the Stochastic GMPEs

Model Type	Large-Magnitude Stress Parameter	Distance Metric	Site Class *	Mean NR (rank)†	Median NR (rank)†	Std NR (rank)†	Median LH (rank)†	Rank†	LLH
Small-magnitude variable stress			EC8	0.595 (C)	0.488 (B)	1.330 (C)	0.401 (A)	C	2.856
	Stress 10 MPa	R_{rup}	FR	0.041 (A)	0.037 (A)	1.145 (B)	0.515 (A)	B	2.272
			RS	0.226 (A)	0.140 (A)	1.139 (B)	0.501 (A)	B	2.299
		R_{rup}	EC8	0.615 (C)	0.490 (B)	1.341 (C)	0.396 (B)	C	2.896
	Stress 5 MPa	R_{rup}	FR	0.046 (A)	0.007 (A)	1.155 (B)	0.503 (A)	B	2.289
		R_{rup}	RS	0.235 (A)	0.150 (A)	1.147 (B)	0.494 (A)	B	2.314
		R_{JB}	RS	0.232 (A)	0.138 (A)	1.102 (A)	0.509 (A)	A	2.241
		R_{hypo}	RS	0.244 (A)	0.164 (A)	1.125 (A)	0.497 (A)	A	2.281
		R_{epi}	RS	0.235 (A)	0.159 (A)	1.095 (A)	0.509 (A)	A	2.230
	Stress 5 MPa (HR‡)	R_{rup}	RS	0.417 (B)	0.353 (B)	1.152 (B)	0.483 (A)	B	2.409
		R_{JB}	RS	0.408 (B)	0.329 (B)	1.098 (A)	0.505 (A)	B	2.316
			EC8	0.698 (C)	0.572 (C)	1.349 (C)	0.378 (B)	C	2.989
	Stress 2.5 MPa	R_{rup}	FR	0.122 (A)	0.081 (A)	1.159 (B)	0.495 (A)	B	2.305
			RS	0.314 (B)	0.221 (A)	1.154 (B)	0.481 (A)	B	2.357
Small-magnitude constant stress		R_{rup}	EC8	−0.268 (B)	−0.349 (B)	1.311 (C)	0.371 (B)	C	2.616
	Stress 10 MPa	R_{rup}	FR	−0.847 (D)	−0.865 (D)	1.195 (B)	0.300 (B)	D	2.873
		R_{rup}	RS	−0.654 (C)	−0.682 (C)	1.107 (A)	0.361 (B)	C	2.518
		R_{rup}	EC8	−0.039 (A)	−0.129 (A)	1.326 (C)	0.386 (B)	C	2.595
	Stress 5 MPa	R_{rup}	FR	−0.630 (C)	−0.667 (C)	1.191 (B)	0.368 (B)	C	2.635
		R_{rup}	RS	−0.434 (B)	−0.480 (B)	1.121 (A)	0.409 (A)	B	2.368
		R_{rup}	EC8	0.164 (A)	0.075 (A)	1.319 (C)	0.407 (A)	C	2.601
	Stress 2.5 MPa	R_{rup}	FR	−0.424 (B)	−0.485 (B)	1.173 (B)	0.428 (A)	B	2.448
		R_{rup}	RS	−0.229 (A)	−0.279 (B)	1.119 (A)	0.447 (A)	B	2.266

NR, normalized residuals; LH, likelihood; LLH, log likelihood.
*Site classification schemes: FR, flat response; RS, reference stations.
†The ranking categories are those defined in Scherbaum *et al.* (2004).
‡HR, model for hard-rock conditions.

et al. (2013) used a variable stress parameter model that was based on observed data from stable continental regions, and they also used a constant stress parameter model. Edwards and Fäh (2013) used various variable stress parameter models, varying the large-magnitude level and the magnitude cutoff. The uncertainty associated with the models is estimated in two different ways. Rietbrock *et al.* (2013) propagated the uncertainties on the input parameters in the simulations, whereas Edwards and Fäh (2013) used only median input parameters and subsequently determined the uncertainty by analysis of the residuals based on the recorded data in Switzerland. Cauzzi *et al.* (2015) performed a regression analysis on the stochastic simulation results of Edwards and Fäh (2013) to build a GMPE given a functional form. They only report modeling uncertainties and suggest using the uncertainty given in Edwards and Fäh (2013) to compute the uncertainty of the Swiss GMPE. Also, the site conditions are slightly different in the two models. Rietbrock *et al.* (2013) used $V_{S30} = 2300$ m/s, whereas Edwards and Fäh (2013) and Cauzzi *et al.* (2015) used $V_{S30} = 1105$ m/s. The standard deviations, which are an important part of the models, have already been compared above, and thus we focus here on the medians.

Figures 14 and 15 compare the stochastic model developed for France in the present study with the stochastic models for the United Kingdom (constant and variable stress parameter models) and with the Swiss stochastic model, for a stress parameter of 6 MPa, which is the suggested best value by Edwards and Fäh (2013) and Cauzzi *et al.* (2015). Regarding the large uncertainties in the estimation of the input parameters from the analysis of the weak-motion data, the different assumptions, and the different predictive variables (distance and site, in the present case), there is good agreement between the model characteristics. The spread in the median predictions is similar to that which is observed in comparisons of empirical GMPEs.

Our model and the Rietbrock *et al.* (2013) model are quite different for large magnitude at short distances (below 20 km) and for small magnitudes at short and long distances. The near-fault attenuation is much stronger in the Rietbrock *et al.* (2013) model, but it shows a slower attenuation with distance, which is further enhanced by the segmented geometrical attenuation model they used. The magnitude scaling is, on the other hand, stronger in our model, regardless of the distance. We believe that the differences are not only due to the difference in rock-site conditions (hard rock versus rock) because Figure 10 shows that there is little difference between the models derived for the two rock conditions. Rather it may be linked with regional attenuation characteristics because the United Kingdom can be classified as a stable continental region, whereas the Alps region is a more active one.

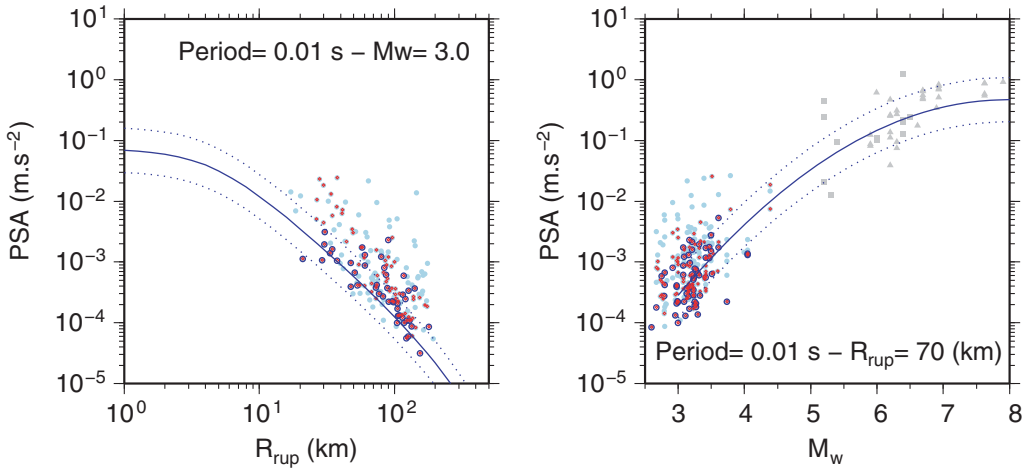

Figure 13. Comparison of the regional stochastic GMPEs (median and median$\pm\sigma$, blue lines) using the variable stress model (plateau value of 10 MPa), with recorded data (light blue dots, EC8 class A sites; open blue circles, stations with flat responses; red diamonds, reference sites from Drouet *et al.* (2010); gray squares, Reference Database for Seismic Ground Motion in Europe (RESORCE) data with $V_{S30} \geq 750$ m/s; gray triangles, NGA data with $V_{S30} \geq 750$ m/s).

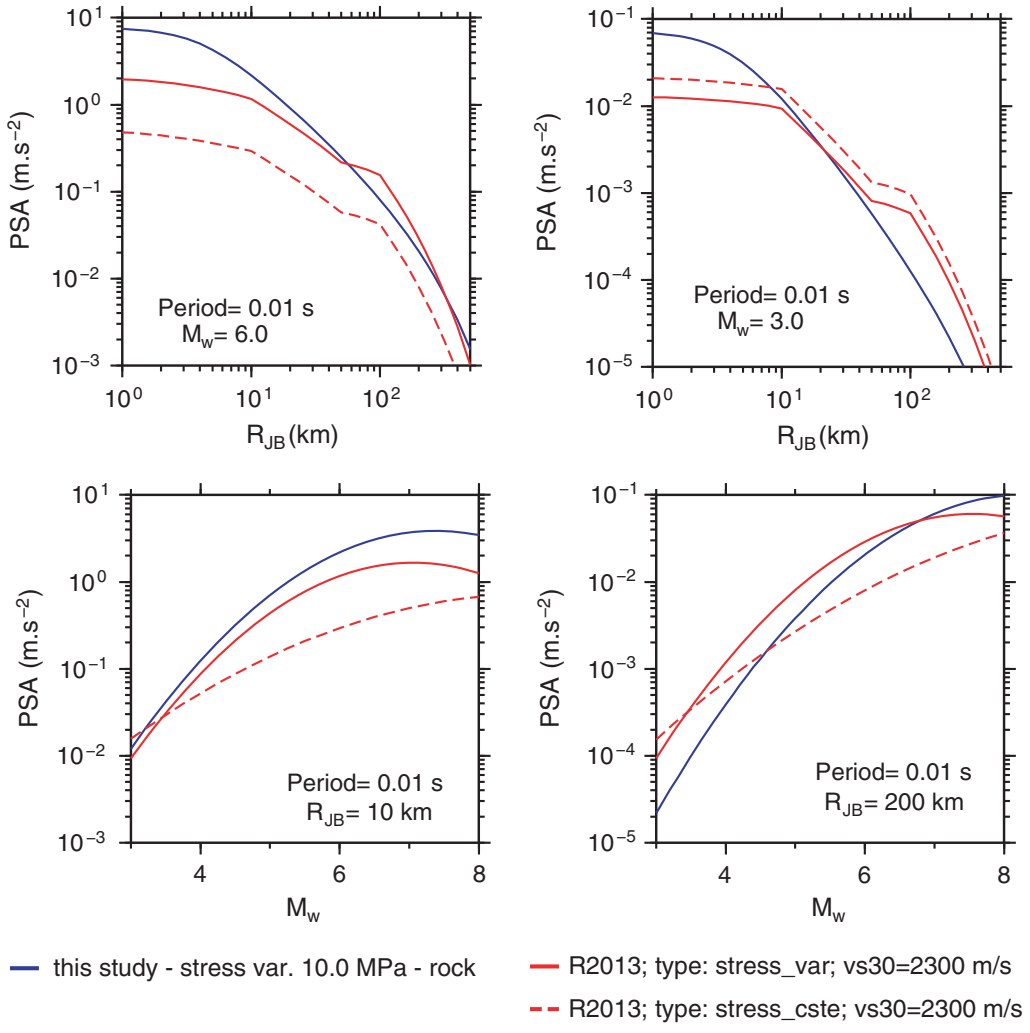

Figure 14. Comparison of stochastic model for the United Kingdom (Rietbrock *et al.*, 2013) and the model derived in this study using variable stress drop with a plateau of 10 MPa for rock sites.

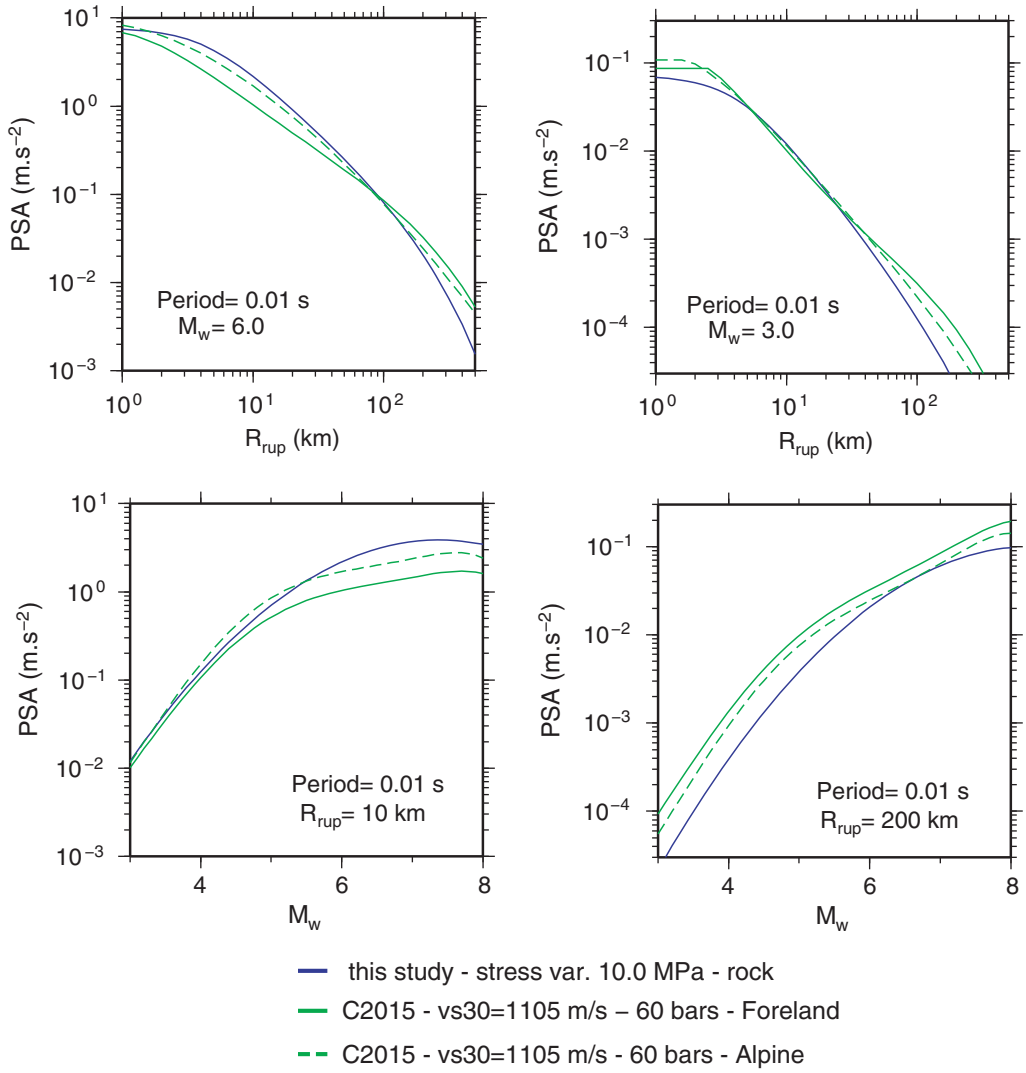

Figure 15. Comparison of stochastic models for Switzerland (Edwards and Fäh, 2013; Cauzzi *et al.*, 2015) and the model derived in this study using variable stress drop with a plateau of 10 MPa for rock sites.

The model for Switzerland uses only a variable stress model but presents two versions, one for the Foreland region and the other for the Alpine region of Switzerland (Edwards and Fäh, 2013). Although Edwards and Fäh (2013) also used a segmented geometrical spreading model, the variations with distance have been smoothed by the regression using polynomial distance terms in Cauzzi *et al.* (2015). The models for Switzerland present a very good agreement with that of this article; both distance and magnitude scaling are very similar. We also note that our model is closer to the Alpine version of the model for Switzerland, which makes sense because the regions analyzed in the two studies are neighboring.

Discussion and Conclusions

Regional stochastic GMPEs have been developed for a broad magnitude range (M_w 3–8) for the French Alps. The models were built in two steps: first, synthetic ground-motion data was computed using SMSIM (Boore, 2003), based on a set of seismological parameters determined from the Fourier spectral analysis of regional data and second, the synthetic data were regressed to build the GMPE.

Most of the input parameters were taken from Drouet *et al.* (2010). Their stress parameter values are used with the results of Drouet *et al.* (2011) to build a stress parameter model which increases with magnitude up to a cut-off magnitude (M_w 4.6), above which stress drop remains constant. Three levels of the plateau value for large magnitude are tested (2.5, 5, and 10 MPa). These levels are supposed to represent average stress-drop levels for large earthquakes (Kanamori and Anderson, 1975; Allmann and Shearer, 2009). The attenuation parameters are also taken from Drouet *et al.* (2010), but a bootstrap technique was used to better characterize the uncertainties of those parameters. Two site conditions are considered: standard-rock sites (V_{S30} = 800 m/s and κ = 0.03 s) and hard-rock sites

($V_{S30} = 2000$ m/s and $\kappa = 0.01$ s), using generic rock amplification curves (Boore and Joyner, 1997; Cotton *et al.*, 2006) and V_{S30}–κ correlation (Van Houtte *et al.*, 2011). Additionally, a duration model is built using the same dataset as used in Drouet *et al.* (2010).

Stochastic simulations are carried out using SMSIM (Boore, 2003), which uses a point-source model, but the effective distance adjustment allows extended fault effects to be mimicked, along with near-source attenuation. Time-domain simulations are used, as opposed to the random vibration theory option that is also available in SMSIM (see Boore, 2003). Simulations were carried out for M_w 3–8, epicentral distances from 1 to 250 km, and 20 spectral periods between 0.01 and 3 s, as well as for PGA and PGV. For each simulated magnitude, 40 earthquake scenarios were constructed, varying the fault orientations and dimensions (completely random due to the lack of information about focal mechanisms in France), the hypocenter depth using a simplified distribution based on observed depths in the Alps, and the hypocenter location on the fault (note that this information is only used to compute the different distance metrics), as well as the stress parameter. For each record simulated, random attenuation parameters, site amplification, κ values, and durations were selected.

All of the parameters used as input in the stochastic simulations are considered as random variables, and the uncertainty is propagated to the synthetic ground motion through random sampling of the input parameter distributions. One critical aspect of this study is the standard deviations used for the input parameters. We tried to base our choices on observations, that is, the results of Cotton *et al.* (2013) for the stress parameter or on observed data for the site condition and duration. There is, of course, some subjectivity in those choices. However, the standard deviations that are coming out of our stochastic GMPEs are consistent with those from empirical GMPEs, and testing our GMPE against various data gives good results.

Sensitivity analysis was carried out to understand the influence of the uncertainty on each input parameter to the total GMPE standard deviation. This sensitivity analysis is complementary to the Molkenthin *et al.* (2014) study, which analyzed the influence of each seismological parameter on the response spectra amplitude. Here, we focus on the uncertainties for the same parameters. The major contributors to the total uncertainty are the stress parameter model and the site model (both site amplification and κ). The uncertainties for the attenuation parameters have second-order influence, and those linked with duration, fault orientation, and hypocenter location are negligible compared to the others. Stress parameter uncertainty directly maps into between-event variability, whereas the uncertainties of the other parameters mainly influence the within-event term. The simulated total ground-motion standard deviation is comparable to that obtained in empirical GMPEs (especially those that include small-magnitude events) under the ergodic assumption (variability of ground motion, including various sites and various sources, Al Atik *et al.*, 2010).

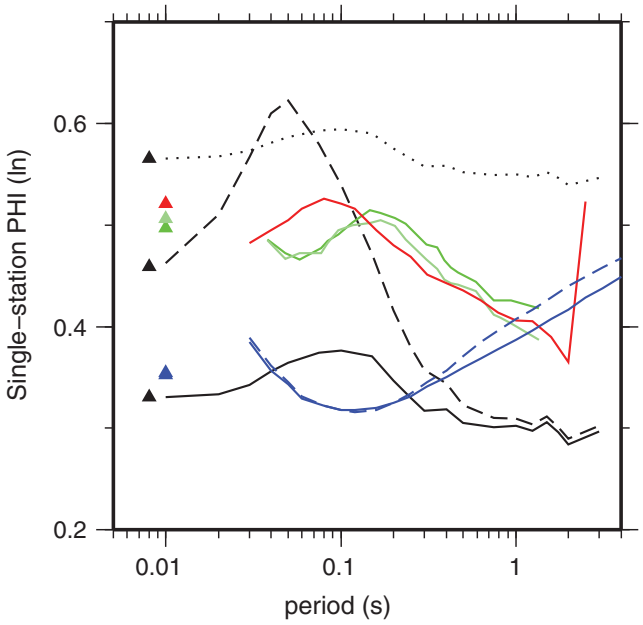

Figure 16. Single-station within-event standard deviation from Rodriguez-Marek *et al.* (2011) (green), Edwards and Fäh (2013) (red), and Rietbrock *et al.* (2013) for the constant stress parameter model (solid blue curve) and the variable stress parameter model (dashed blue curve) compared to the results of this study: within-event variability when the effect of the kappa variability has been removed (dotted black line), within-event variability when the effect of the generic amplification variability has been removed (dashed black line), and within-event variability when both the κ and the generic amplification variabilities have been removed (solid black line).

Al Atik *et al.* (2010) showed that the single-station sigma (the standard deviation of the ground motion at a single site) can be used as a lower-bound value to the standard deviation that would be used in site-specific probabilistic seismic-hazard analysis (PSHA). Rodriguez-Marek *et al.* (2011) and Edwards and Fäh (2013) computed single-station sigmas made up of single-station within-event (ϕ_{SS}) and between-event (τ) terms. The ϕ_{SS} terms are compared in Figure 16, together with the within-event terms from Rietbrock *et al.* (2013). Because Rietbrock *et al.* (2013) did not consider uncertainty for the site term input to the simulations, their within-event standard deviation can be considered as a lower bound for the ϕ_{SS}. Figure 16 also shows the within-event standard deviations of the Alps model for standard rock, from which the part of the uncertainty propagated through the generic site amplification, or κ (see Fig. 11), or both, has been removed. When both are removed, the amplitude of the within-event term gets close to the within-event term from Rietbrock *et al.* (2013), although the shape is different. This difference can be found in the different attenuation models used: depth-dependent Q and segmented geometrical spreading in Rietbrock *et al.* (2013) and frequency-dependent Q and constant geometrical spreading in this study. Figure 11 shows that besides κ, Q has a strong influence on the shape of the

within-event standard deviation. The results in Figure 16 show that depending on the level of knowledge of the site characteristics, the site-specific standard deviations can be computed using the methodology presented in this study. This result is consistent with studies that have suggested that the GMPEs ground-motion variability estimation may depend on the choice of the site condition proxy (e.g., Chiou *et al.*, 2008).

Parametric GMPEs were built by regression of the synthetic data using a state-of-the-art functional form for the four distance metrics considered: R_{epi}, R_{hypo}, R_{JB}, and R_{rup}. Bommer and Akkar (2012) recommended that GMPEs are developed for at least one extended-fault metric (R_{JB} or R_{rup}) and one point-source metric (R_{epi} or R_{hypo}) for two reasons: not all of the PSHA commercial codes include simulation of fault planes (with is computationally extensive) to use GMPEs with their native distance metric; for rapid ShakeMap estimations, when the fault model is not available, point-source metrics have to be relied upon. Testing using the R_{rup} or R_{JB} distance metrics gives a better fit for the NGA data (lower LLHs; see Table 3), whereas for the RESORCE data, the quality of the fit is almost the same, regardless of the distance metric. This could indicate that the fault models are poorly constrained for the European database, which leads to different qualities of the estimated distances.

The stochastic GMPEs are compared with strong ground motion data from the RESORCE database (Akkar *et al.*, 2014) for the Euro-Mediterranean region and from the PEER NGA database (Chiou *et al.*, 2008), which includes worldwide data, although mainly from California and Taiwan. Statistical analysis of the residuals following the methods of Scherbaum *et al.* (2004, 2009) allowed us to compare the performances of the different versions of the stochastic models (variations in the stress parameters for large events). It appears that a stress parameter of 10 MPa (in conjunction with the values of the other parameters of the model) is a good choice to achieve a good fit between the models and the real data.

The stochastic models are also compared to the small-magnitude data recorded in the French Alps. Because of the poorly known site conditions for the RAP stations, three classifications are used to identify rock sites. The GMPEs using high-constant stress parameter values do not fit well the data that, combined with the previous results, support the variable stress parameter models. Beauval *et al.* (2012) also performed testing using data from France compared to popular empirical GMPEs and identified those leading to the lowest LLH values. The stochastic GMPE developed in the present study leads to even lower LLH values, that is, a better fit. As a result of the testing against both strong-motion and weak-motion data, the best version of the stochastic GMPEs is the one using a variable stress parameter with a plateau at 10 MPa. Ⓔ The coefficients of this model are given in Tables S1–S4 (available in the electronic supplement to this article) for epicentral distance, hypocentral distance, Joyner–Boore distance, and rupture distance, respectively.

In the context of seismic-hazard analysis for France, the parametric models presented in the present study provide user-friendly options for logic-tree branches that are calibrated on locally recorded data in the low-magnitude range and consistent with pan-European models in the large-magnitude range. The methods used to define and calibrate the input parameters probability distributions of these stochastic-based GMPEs may be of interest for ground-motion models developments in moderate seismicity areas where weak-motion data are available.

Data and Resources

The Stochastic-Method SIMulation (SMSIM) program is freely available from David M. Boore's website (http://www.daveboore.com/; last accessed July 2014). Illustrations were made using the open source Generic Mapping Tools programs (http://gmt.soest.hawaii.edu/; last accessed July 2014). The data used in this article are from the French accelerometric network (Réseau Accélérométrique Permanent, http://rap.resif.fr; last accessed June 2015), the Pacific Earthquake Engineering Research–Next Generation Attenuation (PEER NGA) project (http://peer.berkeley.edu/nga/; last accessed July 2014), and the Reference Database for Seismic Ground Motion in Europe (RESORCE; Akkar *et al.*, 2014). The SeIsmic Ground-Motion Assessment (SIGMA) project is available at www.projet-sigma.com (last accessed July 2014).

Acknowledgments

This study was supported by the SeIsmic Ground-Motion Assessment (SIGMA) project. The SIGMA project is funded and supported by Electricité de France (EDF), AREVA, Commissariat à l'Energie Atomique (CEA), and Ente Nazionale per l'Energia Elettrica (ENEL), and the authors would like to warmly thank the coordination team, as well as all the participants in the project, for the stimulating discussions during the project workshops. We would also like to thank the three anonymous reviewers and Associate Editor Hiroshi Kawase for their comments which helped to improve the manuscript.

References

Abrahamson, N., and W. Silva (2008). Summary of the Abrahamson and Silva NGA ground-motion relations, *Earthq. Spectra* **24,** 67–97.

Abrahamson, N. A., and R. R. Youngs (1992). A stable algorithm for regression analyses using the random effect model, *Bull. Seismol. Soc. Am.* **82,** 505–510.

Akkar, S., and J. J. Bommer (2007). Prediction of elastic displacement response spectra in Europe and the Middle East, *Earthq. Eng. Struct. Dynam.* **36,** 1275–1301.

Akkar, S., and J. J. Bommer (2010). Empirical equations for the prediction of PGA, PGV and spectral accelerations in Europe, the Mediterranean region and the Middle East, *Seismol. Res. Lett.* **82,** 195–206.

Akkar, S., M. A. SandÄśikkaya, M. Şenyurt, A. A. Sisi, B. O. Ay, P. Traversa, J. Douglas, F. Cotton, L. Luzi, B. Hernandez, and S. Godey (2014). Reference database for seismic ground-motion in Europe (RESORCE), *Bull. Earthq. Eng.* **12,** 311–339, doi: 10.1007/s10518-013-9506-8.

Al Atik, L., N. Abrahamson, J. J. Bommer, F. Scherbaum, F. Cotton, and N. Kuehn (2010). The variability of ground-motion prediction models and its components, *Seismol. Res. Lett.* **81,** 794–801, doi: 10.1785/gssrl.81.5.794.

Allmann, B. P., and P. M. Shearer (2009). Global variations of stress drop for moderate to large earthquakes, *J. Geophys. Res.* **114,** no. B01310, doi: 10.1029/2008JB005821.

Atkinson, G. M., and I. A. Beresnev (1997). Don't call it stress drop, *Seismol. Res. Lett.* **68,** 3–4.

Atkinson, G. M., and D. M. Boore (2006). Earthquake ground-motion prediction equations for Eastern North America, *Bull. Seismol. Soc. Am.* **96,** 2181–2205.

Atkinson, G. M., and D. M. Boore (2011). Modifications to existing ground-motion prediction equations in light of new data, *Bull. Seismol. Soc. Am.* **101,** 1121–1135, doi: 10.1785/0120100270.

Beauval, C., H. Tasan, A. Laurendeau, E. Delavaud, F. Cotton, P. Guéguen, and N. Kuehn (2012). On the testing of ground-motion prediction equations against small-magnitude data, *Bull. Seismol. Soc. Am.* **102,** 1994–2007, doi: 10.1785/0120110271.

Bommer, J. J., and N. A. Abrahamson (2006). Why do modern probabilistic seismic-hazard analyses often lead to increased hazard estimates? *Bull. Seismol. Soc. Am.* **96,** 1967–1977, doi: 10.1785/0120060043.

Bommer, J. J., and S. Akkar (2012). Consistent source-to-site distance metrics in ground-motion prediction equations and seismic source models for PSHA, *Earthq. Spectra* **28,** 1–15.

Bommer, J. J., and A. Martínez-Pereira (1999). The effective duration of earthquake strong-motion motion, *J. Earthq. Eng.* **03,** 127–172, doi: 10.1142/S1363246999000077.

Bommer, J. J., S. Akkar, and S. Drouet (2012). Extending ground-motion prediction equations for spectral accelerations to higher response frequencies, *Bull. Earthq. Eng.* **10,** 379–399, doi: 10.1007/s10518-011-9304-0.

Bommer, J. J., P. J. Stafford, J. E. Alarcón, and S. Akkar (2007). The influence of magnitude range on empirical ground-motion prediction, *Bull. Seismol. Soc. Am.* **97,** 2152–2170.

Boore, D. M. (2003). Simulation of ground motion using the stochastic method, *Pure Appl. Geophys.* **160,** 635–676.

Boore, D. M. (2009). Comparing stochastic point-source and finite-source ground-motion simulations: SMSIM and EXSIM, *Bull. Seismol. Soc. Am.* **99,** 3202–3216.

Boore, D. M., and G. M. Atkinson (2008). Ground-motion prediction equations for the average horizontal component of PGA, PGV, and 5%-damped PSA at spectral periods between 0.01 and 10 s, *Earthq. Spectra* **24,** 99–138.

Boore, D. M., and W. B. Joyner (1997). Site amplifications for generic rock sites, *Bull. Seismol. Soc. Am.* **87,** 327–341.

Boore, D. M., J. P. Stewart, E. Seyhan, and G. M. Atkinson (2014). NGA-West2 equations for predicting PGA, PGV, and 5% damped PSA for shallow crustal earthquakes, *Earthq. Spectra* **30,** 1057–1085, doi: 10.1193/070113EQS184M.

Bora, S., F. Scherbaum, N. Kuehn, and P. Stafford (2014). Fourier spectral- and duration models for the generation of response spectra adjustable to different source-, propagation-, and site conditions, *Bull. Earthq. Eng.* **12,** 467–493, doi: 10.1007/s10518-013-9482-z.

Brune, J. N. (1970). Tectonic stress and the spectra of seismic shear waves from earthquakes, *J. Geophys. Res.* **75,** 4997–5009.

Brune, J. N. (1971). Correction, *J. Geophys. Res.* **76,** 5002.

Cara, M., Y. Cansi, A. Schlupp, P. Arroucau, N. Béthoux, É. Beucler, S. Bruno, M. Calvet, S. Chevrot, A. Deboissy, *et al.* (2015). SI-Hex: A new catalogue of instrumental seismicity for metropolitan France, *Bull. Soc. Géol. France* **186,** 3–19, doi: 10.2113/gssgfbull.186.1.3.

Cauzzi, C., and E. Faccioli (2008). Broadband (0.05 to 20 s) prediction of displacement response spectra based on worldwide digital records, *J. Seismol.* **12,** 453–475.

Cauzzi, C., B. Edwards, D. Fäh, J. Clinton, S. Wiemer, P. Kästli, G. Cua, and D. Giardini (2015). New predictive equations and site amplification estimates for the next-generation Swiss ShakeMaps, *Geophys. J. Int.* **200,** 421–438, doi:10.1093/gji/ggu404.

Chiou, B., R. Youngs, N. Abrahamson, and K. Addo (2010). Ground-motion attenuation model for small-to-moderate shallow crustal earthquakes in California and its implications on regionalization of ground-motion prediction models, *Earthq. Spectra* **26,** 907–926.

Chiou, B. S.-J., and R. R. Youngs (2008). An NGA model for the average horizontal component of peak ground motion and response spectra, *Earthq. Spectra* **24,** 173–215.

Chiou, B. S.-J., R. Darragh, N. Gregor, and W. Silva (2008). NGA project strong-motion database, *Earthq. Spectra* **24,** 23–44.

Cotton, F., R. Archuleta, and M. Causse (2013). What is sigma of the stress drop? *Seismol. Res. Lett.* **84,** 42–48, doi: 10.1785/0220120087.

Cotton, F., G. Pousse, F. Bonilla, and F. Scherbaum (2008). On the discrepancy of recent European ground-motion observations and predictions from empirical models: analysis of KIK-net accelerometric data and point-sources stochastic simulations, *Bull. Seismol. Soc. Am.* **98,** 2244–2261.

Cotton, F., F. Scherbaum, J. J. Bommer, and H. Bungum (2006). Criteria for selecting and adjusting ground-motion models for specific target regions: Application to Central Europe and rock sites, *J. Seismol.* **10,** doi: 10.1007/s10950-005-9006-7.

Douglas, J., and P. Jousset (2011). Modeling the difference in ground-motion magnitude-scaling in small and large earthquakes, *Seismol. Res. Lett.* **82,** 504–508, doi: 10.1785/gssrl.82.4.504.

Drouet, S., M.-P. Bouin, and F. Cotton (2011). New moment magnitude scale, evidence of stress drop magnitude scaling and stochastic ground motion model for the French West Indies, *Geophys. J. Int.* **187,** 1625–1644.

Drouet, S., F. Cotton, and P. Guéguen (2010). V_{S30}, κ, regional attenuation and M_w from small magnitude events accelerograms, *Geophys. J. Int.* **182,** 880–898.

Edwards, B., and D. Fäh (2013). A stochastic ground-motion model for Switzerland, *Bull. Seismol. Soc. Am.* **103,** 78–98.

Edwards, B., D. Faeh, and D. Giardini (2011). Attenuation of seismic shear-wave energy in Switzerland. *Geophys. J. Int.* **185,** 967–984.

Edwards, B., A. Rietbrock, J. J. Bommer, and B. Baptie (2008). The acquisition of source, path, and site effects from microearthquake recordings using Q tomography: Application to the United Kingdom, *Bull. Seismol. Soc. Am.* **98,** 1915–1935, doi: 10.1785/0120070127.

Eurocode 8 (2004). Design of structures for earthquake resistance,—Part 1: General rules, seismic actions and rules for buildings, EN 1998-1, Comité Européen de Normalisation (CEN), Brussels, Belgium.

Fukushima, Y. (1996). Scaling relations for strong ground motion prediction models with m^2 terms, *Bull. Seismol. Soc. Am.* **86,** 329–336.

Hanks, T. C. (1982). f_{max}, *Bull. Seismol. Soc. Am.* **72,** 1867–1879.

Ide, S., G. C. Beroza, S. G. Prejean, and W. L. Ellsworth (2003). Apparent break in earthquake scaling due to path and site effects on deep borehole recordings, *Geophys. Res. Lett.* **108,** 2271, doi: 10.1029/2001JB001617.

Kaklamanos, J., L. G. Baise, and D. M. Boore (2010). Estimating unknown input parameters when implementing the NGA ground-motion prediction equations in engineering practice, *Earthq. Spectra* **27,** 1219–1235.

Kanamori, H., and D. Anderson (1975). Theoritical basis of some empirical relations in seismology, *Bull. Seismol. Soc. Am.* **65,** 1073–1095.

Kempton, J. J., and J. P. Stewart (2006). Prediction equations for significant duration of earthquake ground motions considering site and near-source effects, *Earthq. Spectra* **22,** 985–1013.

Malagnini, L., A. Akinci, R. B. Hermann, N. A. Pino, and L. Scognamiglio (2002). Characteristics of the ground motion in northeastern Italy, *Bull. Seismol. Soc. Am.* **92,** 2186–2204.

Malagnini, L., K. Mayeda, R. Uhrhammer, A. Akinci, and R. B. Hermann (2007). A regional ground-motion excitation/attenuation model for the San Fransisco region, *Bull. Seismol. Soc. Am.* **97,** 843–862.

McGuire, R. K., and T. C. Hanks (1980). rms accelerations and spectral amplitudes of strong ground motion during the San Fernando, California earthquake, *Bull. Seismol. Soc. Am.* **70,** 1907–1919.

Molkenthin, C., F. Scherbaum, A. Griewank, N. Kuehn, and P. Stafford (2014). A study of the sensitivity of response spectral amplitudes on seismological parameters using algorithmic differentiation, *Bull. Seismol. Soc. Am.* **104,** 2240–2252, doi: 10.1785/0120140022.

Pequegnat, C., P. Guéguen, D. Hatzfeld, and M. Langlais (2008). The French accelerometric network (RAP) and national data center (RAP-NDC), *Seismol. Res. Lett.* **79,** 79–89.

Régnier, J., A. Laurendeau, A.-M. Duval, and P. Guéguen (2010). From heterogeneous set of soil data to V_S profile: Application on the French

permanent accelerometric network (RAP) sites, in *Proc. 14 EECE*, Ohrid, Macedonia, 30 August–3 September 2010.

Rietbrock, A., F. O. Strasser, and B. Edwards (2013). A stochastic earthquake ground-motion prediction model for the United Kingdom, *Bull. Seismol. Soc. Am.* **103,** 57–77.

Rodriguez-Marek, A., G. A. Montalva, F. Cotton, and F. Bonilla (2011). Analysis of single-station standard deviation using the KiK-net data, *Bull. Seismol. Soc. Am.* **101,** 1242–1258, doi: 10.1785/0120100252.

Scherbaum, F., F. Cotton, and P. Smit (2004). On the use of response spectral-reference data for the selection and ranking of ground-motion models for seismic-hazard analysis in regions of moderate seismicity: The case of rock motion, *Bull. Seismol. Soc. Am.* **94,** 2164–2185.

Scherbaum, F., E. Delavaud, and C. Riggelsen (2009). Model selection in seismic hazard analysis: An information-theoretic perspective, *Bull. Seismol. Soc. Am.* **99,** 3234–3247, doi: 10.1785/0120080347.

Scotti, O., D. Baumont, G. Quenet, and A. Levret (2004). The French macroseismic database sisfrance: Objectives, results and perspectives, *Ann. Geophys.* **47,** 571–582.

Stafford, P. J. (2014). Crossed and nested mixed-effects approaches for enhanced model development and removal of the ergodic assumption in empirical ground-motion models, *Bull. Seismol. Soc. Am.* **104,** 702–719, doi: 10.1785/0120130145.

Sue, C., F. Thouvenot, and J. Fréchet (1999). Widespread extension in the core of the western Alps revealed by earthquake analysis, *J. Geophys. Res.* **104,** 25,611–25,622.

Toro, G. R., N. A. Abrahamson, and J. F. Schneider (1997). Model of strong ground motions for earthquakes in central eastern North America: Best estimates and uncertainties, *Seismol. Res. Lett.* **68,** 41–57.

Van Houtte, C., S. Drouet, and F. Cotton (2011). Analysis of the origins of (kappa) to compute hard rock to rock adjustment factors for GMPEs, *Bull. Seismol. Soc. Am.* **101,** 2926–2941, doi: 10.1785/0120100345.

Wells, D. L., and K. J. Coppersmith (1994). New empirical relationships among magnitude, rupture length, rupture width, rupture area, and surface displacement, *Bull. Seismol. Soc. Am.* **84,** 974–1002.

Observatório Nacional
Rua General José Cristino 77
Rio de Janeiro, RJ, CEP 20921-400
Brazil
stephane@on.br
(S.D.)

GFZ German Research Center for Geosciences
Telegrafenberg
14473 Potsdam, Germany
fcotton@gfz-potsdam.de
(F.C.)

Manuscript received 10 August 2014;
Published Online 7 July 2015